

Urban aerosol, its radiative and temperature response in comparison with urban canopy effects in megacity based on COSMO-ART modeling

Natalia Chubarova ^{a,*}, Elizaveta Androsova ^{a,b}, Alexander Kirsanov ^{b,d},
Mikhail Varentsov ^{c,d,b}, Gdaliy Rivin ^{b,a}

^a Faculty of Geography, Lomonosov Moscow State University, 119991 Moscow, Russian Federation

^b Hydrometeorological Center of Russia, 123242 Moscow, Russian Federation

^c Research Computing Center of Lomonosov Moscow State University, 119234 Moscow, Russian Federation

^d Russian State Hydrometeorological University, 195196 Saint-Petersburg, Russian Federation

ARTICLE INFO

Keywords:

Urban aerosol pollution
Effective radiative forcing
Aerosol radiative effect
Urban heat island (UHI)
AOD
PM₁₀

ABSTRACT

The study of urban aerosol and its influence on radiation and meteorological regime is important due to the climate effect. Using COSMO-ART model with TERRA_URB parameterization, we estimated aerosols and their radiative and temperature response at different emission levels in Moscow. Mean urban aerosol optical depth (AOD) was about 0.029 comprising 20–30% of the total AOD. Urban black carbon mass concentration and urban PM₁₀ accounted for 86% and 74% of their total amount, respectively. The urban AOD provided negative shortwave effective radiative forcing (ERF) of -0.9 W m^{-2} at the top of the atmosphere (TOA) for weakly absorbing aerosol and positive ERF for highly absorbing aerosol. Urban canopy effects decreased surface albedo from 19.1% to 16.9%, which resulted in positive shortwave ERF at TOA, while for longwave irradiance negative ERF was observed due to additional emitting of urban heat. Air temperature at 2 m decreased independently on the ERF sign, partially compensating (up to 0.5 °C) for urban heat island effect (1.5 °C) during daytime. Mean radiative atmospheric absorption over the Moscow center in clear sky conditions reaches 4 W m^{-2} due to urban AOD. The study highlights the role of urban aerosol and its radiative and temperature effects.

Abbreviations: AOD, aerosol optical depth; PM₁₀, mass concentration of particulate matter with an aerodynamic diameter of 10 µm or smaller; BC, equivalent black carbon mass concentration; SSA, single scattering albedo; UHI, urban heat island; TOA, top of the atmosphere; BOA, bottom of the atmosphere; EDGAR, Emissions Database for Global Atmospheric Research; TNO, Netherlands Organization for Applied Scientific Research; EMEP, European Monitoring and Evaluation Programme; CAMS, Copernicus Atmosphere Monitoring Service; AERONET, Aerosol Robotic Network; COSMO-ART, Consortium for Small-scale Modeling, Aerosols and Reactive Trace gases; CAMS-REG, the Copernicus Atmosphere Monitoring Service regional inventory; ECLIPSE, Evaluating the Climate and Air Quality Impacts of Short-Lived Pollutants; OSM, OpenStreetMap; ECCAD, Emissions of atmospheric Compounds and Compilation of Ancillary Data; ERF, effective radiative forcing; ARE, aerosol radiative effect; MSU MO, Moscow State University Meteorological Observatory..

* Corresponding author.

E-mail address: chubarova@geogr.msu.ru (N. Chubarova).

<https://doi.org/10.1016/j.uclim.2023.101762>

Received 29 May 2023; Received in revised form 8 November 2023; Accepted 9 November 2023

Available online 25 November 2023

2212-0955/© 2023 Elsevier B.V. All rights reserved.

1. Introduction

The importance of the study of anthropogenic aerosol pollution is related to its impact on the radiation and meteorological regime of the atmosphere and on climate, which is noted in various international assessment reports and papers (Duarte and Duarte, 2020; IPCC, 2023, 2014; Jacobson, 1998; Wang et al., 2020; Zhdanova et al., 2020; Zhuang et al., 2018). Depending on its composition and properties, anthropogenic aerosol may differently affect atmospheric radiation and change meteorological regime of the atmosphere (Bond et al., 2013; Chou et al., 2006; Crutzen, 2004; Kirsanov et al., 2020; Liu et al., 2019; Tsikerdekis et al., 2019).

Usually, aerosol urban modeling is carried out on the basis of specified emissions of pollutants according to different inventories, for example, EDGAR (Emissions Database for Global Atmospheric Research), TNO (Netherlands Organization for Applied Scientific Research), EMEP (European Monitoring and Evaluation Programme), CAMS (Copernicus Atmosphere Monitoring Service) (Gliß et al., 2021; IPCC, 2023; Kuenen et al., 2022, 2014). The emissions of aerosol precursors and primary aerosol may significantly differ in these datasets. The values of simulated aerosol parameters and aerosol concentrations obtained according to these inventories should be accurately tested (Dinkelacker, 2023; Schutgens et al., 2020) against observations, using ground-based or satellite data (Chubarova et al., 2020; Zawadzka et al., 2013; Zhdanova et al., 2020).

Indeed, urban air pollution and urban-induced meteorological effects are the most obvious examples of anthropogenic modification of atmospheric properties (Crutzen, 2004; Oke et al., 2017). These effects typically coexist in the cities simultaneously, so their mutual influence may be expected (Jacobson, 1998; Yu et al., 2020). However, their relationships are not well understood. The most studied feature of urban climate is the urban heat island (UHI), i.e., a temperature increase in the cities with respect to surrounding rural or natural areas due to human activities and urban land cover modifications (Oke et al., 2017). Aerosols may reduce or enhance the UHI depending on their properties and meteorological conditions (Crutzen, 2004; Jacobson, 1998). However, there are only a few studies concerning the comparisons of the UHI and its offset by aerosol in large cities. According to the Weather Research and Forecasting (WRF) model for heavily polluted cities (Beijing and New York City), Jin et al. (2010) obtained temperature decrease of 0.5 °C–1 °C using the observed aerosol optical depth (AOD) of upper quartile. The urbanization and aerosols were also investigated during a typical winter haze event in Beijing using the Rapid-Refresh Multiscale Analysis and Prediction System – Short Term (RMAPS-ST) (Yu et al., 2020). According to this study the aerosols reduced urban-related warming during the daytime by 20% with the increase in PM_{2.5} from 200 to 400 µg m⁻³. In some conditions aerosol can, on the contrary, enhance urban heat island during night (Cao et al., 2016). Folberth et al. (2012) described the influence of megacities on air quality and radiative forcing on a global scale with the negative estimates of about -6 W m⁻² in shortwave and + 1.5 W m⁻² in longwave irradiance.

For the Moscow region, Chubarova et al. (2022) obtained model estimates of aerosol pollution, using the TNO emission data (Kuenen et al., 2014; Pulles et al., 2007) embedded in the COSMO-ART (Consortium for Small-scale Modeling; Aerosols and Reactive Trace gases) model system (Baldauf et al., 2011; Kuznetsova et al., 2022; Rivin et al., 2019; Vil'fand et al., 2017; Vogel et al., 2010). However, the numerical experiments in this study were based on the very low, close to zero, lateral boundary conditions of the domain providing only the estimation of the urban aerosol component. This did not allow us to calculate radiation and temperature effects. Due to the coarse 7 km model grid step (Chubarova et al., 2022), the main focus of the study was aimed at the differences between observations in the city, at the Moscow State University Meteorological Observatory (MSU MO) and in suburbs in Zvenigorod. In addition, the previous studies for Moscow did not take into account for the specific features of urban canopy, their impacts on atmospheric processes and atmospheric composition.

The aim of this paper was to estimate urban aerosol at surface and in the atmospheric column in Moscow megacity, to study its radiative and temperature feedbacks, and to compare them with urban canopy effects, i.e. the physical effects induced by the presence of the urban environment with buildings, roads, etc., including the UHI. For this purpose we performed numerical experiments with the COSMO-ART mesoscale non-hydrostatic model system (Baldauf et al., 2011; Rivin et al., 2020, 2019), online-integrated with the ART chemical transport model (Vil'fand et al., 2017; Vogel et al., 2010) with the modern up-to-date inventory CAMS-REG (the Copernicus Atmosphere Monitoring Service regional inventory) and ECLIPSE (Evaluating the Climate and Air Quality Impacts of Short-Lived Pollutants) databases on pollutant emission substances (Kuenen et al., 2022; Stohl et al., 2015), as well as with the TERRA_URB urban parameterization (Garbero et al., 2021; Wouters et al., 2016). Several numerical experiments at a 2 km grid step with different levels of emissions including the emissions with the enhanced black carbon (BC) ratio provide the estimates of the sensitivity of solar radiation and meteorological characteristics to different aerosol properties.

2. Materials and methods

The analysis of aerosol pollution and its radiative and meteorological effects was carried out for Moscow, which is one of the world's largest cities with the area of >2500 km² and population of >13.0 million. Moscow has a developed industrial infrastructure and a wide network of highways with about 4.4 million of automobiles with 90% of passenger cars (Kulbachevsky, 2022). This provides a significant influence on the level of urban emission in the city area.

For assessing the aerosol effects on radiative and meteorological parameters, it is necessary to adequately reproduce aerosol columnar properties, mainly, aerosol optical depth and single scattering albedo. The correct description of aerosol phase function, is not so important (Liou, 2010). However, in some specific conditions, as winter haze in China, aerosol phase function may noticeably alter due to hydroscopic growth of aerosol (Zhang et al., 2021). The evaluation of these parameters depends on specific emissions of aerosol gas-precursors, primary aerosol, and on meteorological characteristics (wind velocity, relative humidity, temperature, and the stratification of the atmosphere). Since aerosol particles play negative effects on human health (Carey et al., 2016; Lu et al., 2015; Manosalidis et al., 2020; Revich, 2018), we also analyze mass concentration of particulate matter with an aerodynamic diameter of 10

μm or smaller (PM_{10}) at surface level focusing on their spatial distribution in Moscow. A more detailed model description with specifications concerning the configuration of the model, the description of the emissions and observations used for the analysis and for model testing are given in the subsections below.

2.1. Model configuration, pollutant emissions specification and numerical experiments description

For studying urban aerosol effects and evaluating sensitivity of radiative and meteorological characteristics to different urban aerosol properties, we used a regional non-hydrostatic COSMO model of the atmosphere (<http://www.cosmo-model.org/>) online integrated with interactive chemical transport ART model. The COSMO model is being developed by the international consortium led by the German Weather Service (Deutsche Wetterdienst) (Baldauf et al., 2011) and is used for numerical weather forecasting objectives in a number of countries around the world, including the COSMO-Ru system at the Hydrometeorological Center of Russia (Rivin et al., 2019). The ART chemical transport model describes such processes as chemical reactions, photodissociation, coagulation, condensation, nucleation, precipitation, dry and wet deposition, and also takes into account interactive influence of aerosol on radiative and meteorological characteristics (Vogel et al., 2009, 2010). The calculations of reactive gaseous and particulate matter are based on the enhanced KAMM/DRAIS/MADEsoot/-dust model (Riemer et al., 2003; Vogel et al., 2010). For radiative simulations a delta-two-stream radiative algorithm was used (Ritter and Geleyn, 1992) for estimating shortwave (from $0.25 \mu\text{m}$ to $4.64 \mu\text{m}$) and longwave (from $4.64 \mu\text{m}$ to $104.5 \mu\text{m}$) radiation. In the algorithm the spectrum is divided into three intervals in the solar spectrum with effective wavelengths of 500, 880, and 2000 nm, and into five intervals in the far-infrared spectrum. Its testing against aerosol and radiation measurements at the MSU MO has revealed uncertainties of about 2–3% in calculating net shortwave radiation under clear sky conditions (Poliukhov et al., 2017).

In the Hydrometeorological Center of Russia, the COSMO-ART system is used for operational forecasts of the concentrations of different pollutants over the territory of the Moscow region (Kuznetsova et al., 2022; Vil'fand et al., 2017). In addition, COSMO model is used for a number of research tasks related to, for example, evaluation of urban aerosol (Chubarova et al., 2022) and the effect of aerosol on weather conditions (Kirsanov et al., 2020).

To represent the specific features of the urban-atmosphere interaction, the COSMO model was supplemented by the TERRA_URB urban land surface parameterization (Garbero et al., 2021; Wouters et al., 2016). This is a simple but computationally efficient bulk parameterization, which brings canopy-dependent urban physics to standard parameters used by TERRA land surface model (heat capacity, heat conductivity, roughness length, reflectivity, and emissivity) in accordance with semi-empirical dependencies of these characteristics on the geometric urban canopy parameters. It also takes into account the soil sealing by artificial impervious surfaces and anthropogenic heat release. Previously, the TERRA_URB scheme has proven itself well in the tasks of the regional climate modeling (Varentsov et al., 2020, 2018) and numerical weather forecast (Rivin et al., 2020, 2019) for Moscow region, and demonstrated its ability to capture urban-induced effects at surface and boundary layers including heat island (Garbero et al., 2021; Varentsov et al., 2020), urban-induced anomalies of humidity, wind and precipitation (Varentsov et al., 2018). However, TERRA_URB has been never used together with the ART scheme due to incompatibility of these modules in the previous COSMO versions. This problem was solved only in the latest COSMO version 6.0. In our study, this new version of the COSMO model is used for the first time to simulate the processes in the urban atmosphere with the simultaneous application of the urban parameterization and online coupled interactive chemical transport model.

2.1.1. Model configuration

Within the framework of numerical experiments, the COSMO model system was used for dynamic detail elaboration of ERA5 (ECMWF Reanalysis v5) global atmospheric reanalysis with a grid step of approximately 31 km (Hersbach et al., 2020) for the Moscow region using two nested domains: external with a grid step of 7 km with a size of 160×160 cells ($1100 \times 1100 \text{ km}$), and internal one with a grid step of 2 km with the size of 300×300 cells ($600 \times 600 \text{ km}$). The lateral boundary conditions for the outer region were updated every hour according to the reanalysis data. In addition, the spectral nudging method (von Storch et al., 2000) was used, providing the assimilation of large-scale components of atmospheric circulation according to reanalysis data within the modeling domain. Spectral nudging was applied to the fields of temperature and horizontal components of wind velocity starting from the isobaric surface of 850 hPa. The results of calculations for the outer domain acted as boundary conditions for the inner one. The initial conditions for the active land layer were set for both domains according to the analysis of the German weather service ICON (Icosahedral Nonhydrostatic Weather and Climate Model) model with a grid step of 13 km. Test calculations have shown that this approach (setting lateral boundary conditions according to ERA5 data and initial ones according to ICON model) provides the best reproduction of temperature and humidity conditions (Varentsov et al., 2023). The configuration of the physical block of the model took into account the experience of previous studies for the Moscow region (Garbero et al., 2021; Varentsov et al., 2020). It included the use of a new scheme of vertical diffusion in the boundary layer of the atmosphere (loldtur = false), new parameterizations of evaporation from open soil and heat exchange of the atmosphere with the plant canopy (itype_evl = 4, itype_canopy = 2) (Schulz and Vogel, 2020), exponential profile of the plant root density distribution in the soil (itype_root = 2) and increasing the default plant root depth by 2.5 times.

The TERRA_URB parameterization was used for the inner domain. The external urban canopy parameters of the urban environment necessary for the TERRA_URB scheme (spatial distribution of surface imperviousness, geometric, thermophysical and radiation properties of buildings, annual-mean anthropogenic heat flux) were set using the original methodology from (Samsonov and Varentsov, 2020; Varentsov et al., 2020) based on OpenStreetMap (OSM) open cartographic data, map of Local Climate Zones (Stewart and Oke, 2012) available for Moscow from (Samsonov and Trigub, 2018; Varentsov et al., 2020) and global raster databases on the

types of land cover Copernicus Global Land Cover and (Buchhorn et al., 2020) and ESA WorldCover (Zanaga et al., 2021). Based on OpenStreetMap data we also estimated the area fractions occupied by roads and industrial territories, which were used to correct the spatial distribution of emissions, as described below. The spatial distribution of external parameters of the urban environment are shown in Fig. S1. This detailed approach was applied for the central part of the inner model domain with the size of 200×200 km. Outside this area model's default description of urban areas was used.

2.1.2. Methodology for pollutant emissions specification

For assessing atmospheric radiative properties, it was necessary to use realistic aerosol concentrations at the lateral boundaries of the domain and appropriate anthropogenic pollutants emissions. In the previous study (Chubarova et al., 2022), we specified only urban aerosol, which made the analysis of radiative and meteorological feedback not possible. In this work, the CAMS reanalysis data (Giusti, 2022; Inness et al., 2019) was used to set the lateral boundary conditions for evaluation background aerosol advection. As input data on pollutants emissions, we used the regional CAMS-REG dataset with the resolution of about 6 km available at the ECCAD (Emissions of atmospheric Compounds and Compilation of Ancillary Data) service: <https://eccad.aeris-data.fr/>, last access 13/09/2023, Granier et al., 2012). Unfortunately, this dataset does not include the information on black carbon emissions, preventing the account of the aerosol absorbing fraction, which is significant in urban conditions (Chubarova et al., 2022). Therefore, in addition we used the ECLIPSE dataset (<https://iiasa.ac.at/models-tools-data/global-emission-fields-of-air-pollutants-and-ghgs>, last access 15/09/2023). According to it, the BC/PM₁₀ ratio for Moscow is 6%, which is close to the mean BC/PM₁₀ value of about 5% in Moscow, obtained from observations (Chubarova et al., 2021). Note that the application of the TNO2010 and TNO2003-2007 datasets in our previous analysis led to significant overestimation of the BC/PM₁₀ ratio up to 12–18% (Chubarova et al., 2020). These overestimated BC/PM₁₀ values resulted in very low, unrealistic values of single scattering albedo (SSA), which could affect radiative calculations. To eliminate this effect, the BC/PM₁₀ fraction emission ratio was set according to the ECLIPSE data with a slight 1% correction according to the measurements. Black carbon emissions were determined in accordance with this ratio and known PM₁₀ emissions. The most significant sources of pollutants emissions according to the CAMS and ECLIPSE inventories are the industrial sector, road transport and electric energy industry. At the same time, for Moscow, in the CAMS, ECLIPSE and EMEP inventories, aerosol particle emissions from road transport are several times less than those from industry, which is far from reality in the Moscow region. Primary aerosol particles emissions from vehicles occur, when fuel (especially diesel) is burned, as a result of mechanical wear of tires and the roadway. Industrial aerosol emissions are associated with the processes of combustion and processing of raw materials, loading, and unloading of bulk materials, etc. The report on the state of the environment in the city of Moscow in 2021 (Kulbachevsky, 2022) noted that emissions from stationary sources were about 60.000 tons, while emissions of particulate matter were estimated at about 3% of this total, and together with emissions of gaseous volatile organic and liquid compounds comprised 20%. The emissions from motor vehicles are 323.000 tons or 84% of the total amount of major pollutants. At the same time, solid emissions from trucks alone are 60%, or about 194.000 tons (Kulbachevsky, 2022). In the inventories, the total PM₁₀ emissions from motor vehicles are much lower: they are about 30% in the EMEP dataset, and only 4–6% in the CAMS dataset for the Moscow region. At the same time, the emissions from the industrial sector according to the CAMS and ECLIPSE datasets are generally consistent with each other. Therefore, we decided to use the emissions from various sectors, including industry, in accordance with the CAMS data together with significant increase in vehicle emissions (around 80–85% of total emissions for different species responsible for aerosol generation), which is generally consistent with the estimates of relative differences between the emissions from industry and transport according to this new national report (Kulbachevsky, 2022). As a result, all types of the emissions, except road transport ones, were set according to the CAMS dataset with the correction from the ECLIPSE inventory, while the road transport emissions were significantly increased making them comparable with the observed ones in Moscow. Table S1 presents the updated percentage of sectors for emissions of different pollutants, which distribution was modified.

After correction of source sector distribution, spatial distribution of emissions should be changed accordingly, since the 6 km coarse resolution does not describe the road network well enough for the 2 km resolution experiments. Anthropogenic pollutants emissions over the territory of the Moscow region were redistributed in accordance with the OpenStreetMap road transport and industrial area fraction in a grid cell (see Fig.S1) using the equation:

$$v_i = p_i (\Sigma v^* k) / \Sigma p, \quad (1)$$

Here, v_i is the redistributed emission value in the i-th cell separately for road transport and industrial sector, Σv is the sum of initial emission values for industrial sector in the approximately 200×200 km area, where detailed city-descriptive parameters are available, k is the multiplying factor equal to 1 for the industrial sector and 7 for the road transport sector (to account for the corresponding increase in the road-transport emissions), p_i is the area fraction values separately for the road transport and industrial sector in the i-th cell, Σp is the sum separately for road and industrial area fraction values over the 200×200 km area.

Fig. S2 shows the final scheme of the emissions distribution from different sources, which were taken into account in the numerical experiments.

2.1.3. Description of the numerical experiments

Several numerical experiments using the COSMO-ART model system were carried out for evaluating the aerosol properties of the atmosphere, their radiative and temperature effects. In addition, we compared the aerosol radiative and temperature response with the urban canopy effects represented by the TERRA_URB scheme over Moscow. In order to evaluate the effects of different aerosol properties we used various types of urban emissions in the model experiments.

The first type of emissions, shown in Fig.S3, is the modified CAMS-REG inventory dataset with the redistribution of PM₁₀, NO, NO₂, SO₂ according to OSM dataset and increased road transport sector. This type of emissions is marked as the standard emissions in the text below. The second type of emissions is the modified dataset, which was characterized by 3-fold increase of the first type. The third type of emission dataset was also characterized by 3-fold increase of the first type but with significant 30% growth in BC/ PM₁₀ fraction. This 30% limit was taken in accordance with the highest BC/PM₁₀ ratio observed in Moscow (Chubarova et al., 2022). Note, that in the first and the second type of the emissions BC/PM₁₀ ratio was about 5%. Using these datasets as input parameters, we carried out the sensitivity study of radiative and meteorological parameters to different types of emissions in Moscow conditions. We also evaluated the effects with a 3-fold increase in pollutant emissions, providing weakly absorbing aerosol, which is typical in Moscow (Chubarova et al., 2011a; Chubarova et al., 2011b), and highly absorbing aerosol. In this study we define “weakly absorbing” as aerosol single-scattering albedos that exceed 0.7 in visible region of spectrum.

We also made several experiments to assess the role of the urban aerosol generation according to the ART chemical transport module. In order to compare aerosol temperature and radiative response with corresponding urban canopy effects, we performed additional simulations with and without TERRA_URB parameterization. When TERRA_URB parameterization was switched off, the city was represented as a natural vegetated surface. Urban canopy effects on temperature, i.e., the urban heat island, and radiation were estimated as a difference between simulations with and without TERRA_URB. Several experiments were also made for evaluating the role of CAMS boundary conditions to assess the role of aerosol advection, and for estimating the role of the application of Tegen aerosol climatology (Tegen et al., 1997), which is usually utilized in the COSMO model. Table S2 summarizes the information about the nine numerical experiments used in the study including three control experiments without the ART module application. It also includes the short names of the experiments, which are used throughout the study. For evaluating urban aerosol components (AOD, PM₁₀, BC), and aerosol radiative and temperature effects, we estimated the difference between the specified experiments as shown in Table S3. For example, the difference between the A1TU and ctrl_TU experiments (see Table 2S, 3S) provided the estimates of urban aerosol at standard emission level and their effects on radiative and meteorological properties of the atmosphere.

For assessing effective radiative forcing (*ERF*) at the top (TOA) and at the bottom (BOA) of the atmosphere, we used the following equation:

$$ERF(i) = N(i)_{TOA(BOA),urb} - N(i)_{TOA(BOA),no\ urb}, \quad (2)$$

where *N* is net irradiance, index *i* denotes shortwave, longwave, or total spectral range, the index “*urb*” denotes the presence of urban aerosol, the index “*no urb*” denotes the absence of urban aerosol.

For evaluating an aerosol radiative effect (ARE) the following equation is used:

$$ARE(i) = N(i)_{TOA(BOA)} - N(i)_{TOA(BOA),AOD=0} \quad (3)$$

ARE accounts the effects of all urban and background aerosol over Moscow region against the aerosol free atmosphere, while *ERF* characterizes only the effects of urban aerosol.

As a result, a set of the numerical experiments provides us the range of the total aerosol and urban aerosol influence on air temperature, which is compared with the urban heat island estimates.

Direct radiative effects are analyzed in the cloudless atmosphere while in all-sky conditions both direct and possible semi-direct effects could be observed. The indirect aerosol effects on cloudiness are not considered in this study.

The numerical experiments with the COSMO-Ru-ART model system were conducted for the period from April 28th to May 7th, 2019. This period was chosen due to availability of experimental data, large number of cloudless days in Moscow, necessary for AERONET aerosol retrievals (see their description below), and homogeneous surface with grass without snow cover. The analysis was made over the territory of Moscow agglomeration and separately over the MSU MO, where we have the data for testing both surface and columnar aerosol properties.

2.2. Description of experimental dataset

For a detailed testing of the model properties of atmospheric aerosol and its urban component, we used the measurements at the MSU MO (55.7 N, 37.52E). The MSU MO is located close to the center of Moscow at the territory of the MSU Botanical Garden in the park area at several kilometers distance from the local sources of emissions (power stations) and about 300–450 m away from the nearest highway. Hence, it is characterized by a relatively clean atmosphere due to its location in the park zone and belongs to “natural area” in the classification of pollution burden. The measurements include the retrievals of columnar aerosol properties using CIMEL sun/sky photometer, which was operated within the AERONET network (Chubarova et al., 2011a; Holben et al., 1998). In particular, aerosol optical depth at 500 nm, the Angstrom extinction exponent (AEE), single scattering albedo at 675 nm, (Dubovik and King, 2000) from the version 3 level 2 dataset (Giles et al., 2019) were applied for testing model simulations. The data were available with 15 - min resolution during daytime. In addition, for testing the urban component of AOD (Δ AOD), we used similar AERONET measurements at the Zvenigorod Scientific Station of A.M. Obukhov Institute of Atmospheric Physics, Russian Academy of Science (IAP RAS) located 55 km to the west of the MSU MO (55.7°N, 36.8°E). Due to prevailing westerlies and its location far from local anthropogenic emissions, it can be characterized as a background site.

We also used the data from 23 stations of the Mosecomonitoring Agency located at various distances from pollution sources in Moscow with a time resolution of 20 min (Fig.S4). We followed the classification adopted at the Mosecomonitoring Agency, based on location of the sites in the proximity of green zones, parks, residential areas, highways, and industrial enterprises. This classification

consists of four classes: natural area (city background conditions in the proximity of green zones), residential area, the area under the influence of mixed pollution sources, and the area close to highways. In this paper we focused on the analysis of the PM₁₀ aerosol mass concentrations provided by the TEOM 1400a (Thermo Environmental Instruments Inc., USA). BC dataset was provided by Dr. Popovicheva (Popovicheva et al., 2022). Aerosol equivalent black carbon mass concentration was recorded with 1 min resolution using a custom-made portable aethalometer (Popovicheva et al., 2017). The BC concentrations were determined by converting the time-resolved light attenuation to BC mass concentration at 650 nm. Their estimation was characterized by a specific mean mass attenuation coefficient (MAC) (Popovicheva et al., 2017). The calibration parameter for quantification of BC mass concentration was evaluated using parallel long-term measurements against an AE33 aethalometer (Magee Scientific) with high determination coefficient R² = 0.92 (Popovicheva et al., 2022). The uncertainty of BC measurements from both aethalometers depends on the accuracy of the MAC value used for the conversion of the light absorption coefficient to mass concentration. The uncertainties of the reported MAC values remain as high as 30–70% due to the lack of appropriate reference methods. More details can be found in Popovicheva et al. (2022). We also used meteorological observations at the MSU MO, and other standard meteorological stations located on the territory of Moscow and the suburbs.

3. Results

3.1. Aerosol and its radiative and temperature effects at the MSU MO

3.1.1. Aerosol properties

The columnar and surface aerosol characteristics were obtained from different COSMO-ART numerical experiments and from observations separately for clear sky and all-sky conditions (Table 1, Fig. 1).

There is a noticeable difference in simulated aerosol characteristics with a pronounced increase in surface aerosol content and columnar AOD at 3-fold emission rate (#A3CTU, #A3BTU, #A3TU). The A1CTU experiment with standard emissions provides a satisfactory agreement with measurements for PM₁₀, however, slightly underestimates AOD. Almost all aerosol characteristics are

Table 1

The main statistics of aerosol parameters (aerosol optical depth at 550 nm, AOD; single scattering albedo in visible range, SSA; BC, $\mu\text{g m}^{-3}$; PM₁₀, $\mu\text{g m}^{-3}$) and surface albedo (in %) obtained from the numerical experiments with the COSMO-ART model and from measurements in clear sky and all-sky conditions at the MSU MO. April 28th-May 8th, 2019.

Type of experiment or measurements	Parameter	mean	sigma	mean	sigma
		Clear sky (N = 20)	All-sky (N = 239)	Clear sky (N = 20)	All-sky (N = 239)
Conditions					
Measurements	AOD	0.112	0.048	0.14	0.051
	SSA	0.903	0.003	0.941	0.031
	Surface albedo, %	20.8	1.7	19.7	1.6
	BC, $\mu\text{g m}^{-3}$	2.017	2.712	1.307	1.355
	PM ₁₀ , $\mu\text{g m}^{-3}$	25	23	26	17
4 exp. (A1TU)	AOD	0.029	0.014	0.034	0.029
	SSA	0.71	0.018	0.713	0.015
	Surface albedo, %	16.9	0	16.9	0.1
	BC, $\mu\text{g m}^{-3}$	0.801	0.498	1.054	0.691
	PM ₁₀ , $\mu\text{g m}^{-3}$	14	7	19	11
5 exp. (A3TU)	AOD	0.089	0.047	0.101	0.091
	SSA	0.745	0.024	0.749	0.024
	Surface albedo, %	16.9	0	16.9	0.1
	BC, $\mu\text{g m}^{-3}$	2.447	1.563	3.217	2.142
	PM ₁₀ , $\mu\text{g m}^{-3}$	42	23	56	35
6 exp. (A3BTU)	AOD	0.11	0.051	0.144	0.181
	SSA	0.353	0.037	0.364	0.033
	Surface albedo, %	16.9	0	16.9	0.1
	BC, $\mu\text{g m}^{-3}$	15.497	10.314	19.427	12.682
	PM ₁₀ , $\mu\text{g m}^{-3}$	52	26	69	41
7 exp. (A1CU)	AOD	0.086	0.029	0.103	0.045
	SSA	0.669	0.076	0.709	0.076
	Surface albedo, %	16.9	0	16.9	0.1
	BC, $\mu\text{g m}^{-3}$	0.922	0.485	1.241	0.721
	PM ₁₀ , $\mu\text{g m}^{-3}$	19	7	25	11
8exp (A1CTU)	AOD	0.085	0.026	0.104	0.045
	SSA	0.669	0.076	0.709	0.076
	Surface albedo, %	16.9	0	16.9	0.1
	BC, $\mu\text{g m}^{-3}$	0.922	0.485	1.241	0.721
	PM ₁₀ , $\mu\text{g m}^{-3}$	19	7	25	11
9 exp. (A3CTU)	AOD	0.146	0.052	0.176	0.094
	SSA	0.708	0.049	0.738	0.044
	Surface albedo, %	16.9	0	16.9	0.1
	BC, $\mu\text{g m}^{-3}$	2.53	1.538	3.496	2.316
	PM ₁₀ , $\mu\text{g m}^{-3}$	47	22	64	35

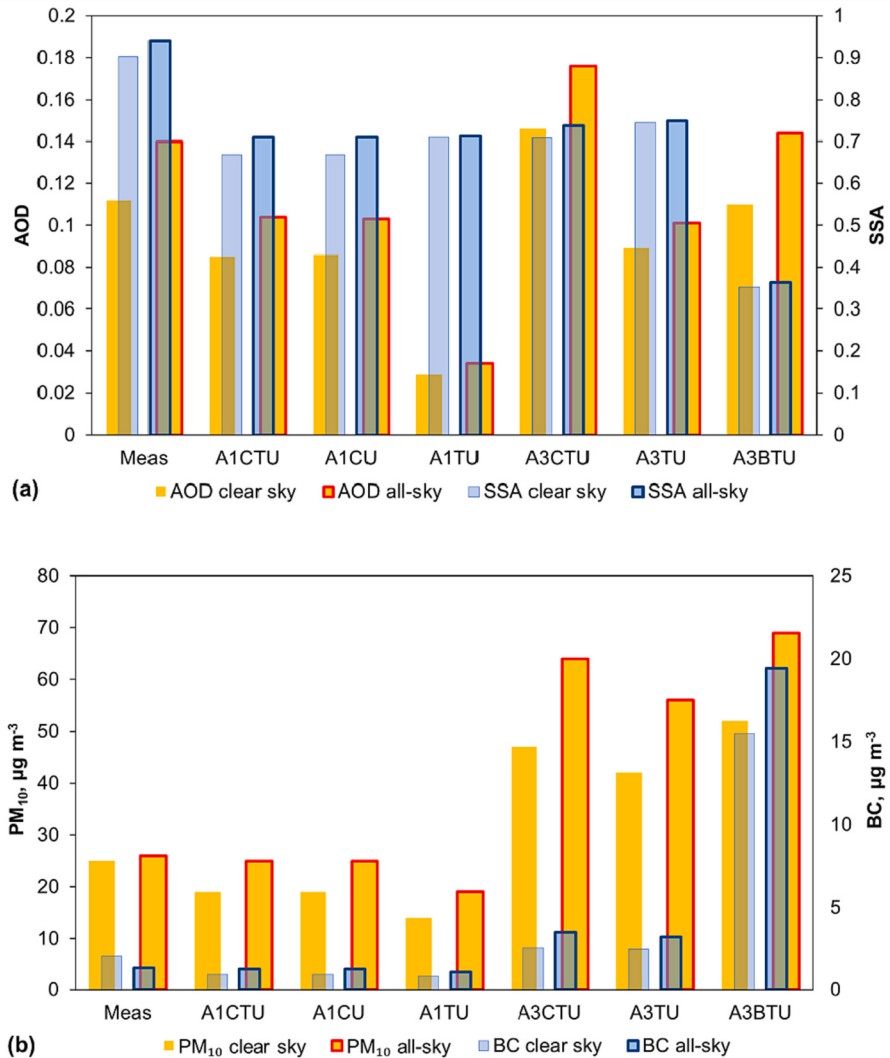


Fig. 1. Mean AOD and SSA columnar aerosol characteristics (a), surface PM₁₀ and BC mass concentrations (b) according to measurements and modeling in different experiments in clear and all-sky conditions. MSU MO. The AOD values are given without accounting the Tegen climatology.

similar in clear sky and all-sky conditions. There is a slight model SSA underestimation in all experiments, which may provide an additional absorption in the atmosphere, however, since AOD is low, the uncertainty in radiation is not very large, comprising 3–4% for global irradiance according to our simulations using the TUV model (Madronich and Flocke, 1999). The modeled BC concentrations at standard emission level for all-sky conditions are in a satisfactory agreement with measurements. Hence, a slight underestimation of SSA might be attributed to a lower content of the other type weakly absorbing aerosol. This slight underestimation of the total aerosol content can be seen in Table 1, comparing measured AOD with the results of the A1CTU and A1CU experiments. Note, that this underestimation does not connect with weakly absorbing sulphate aerosol, since the concentrations of SO₂, which is its precursor, are very low in Moscow (Chubarova et al., 2022). However, a world-wide tendency of sulphate aerosol decreasing (Jin and Pryor, 2020; Jin et al., 2023; Poliukhov et al., 2022) may result in smaller SSA.

A special experiment (A3BTU) with elevated BC emissions provides the SSA estimates up to 0.35 and BC = 15.5 $\mu\text{g m}^{-3}$ characterizing the upper possible BC level, which, however, can be observed in China and India. For example, BC is about 10 $\mu\text{g m}^{-3}$ in urbanized areas of China (Huang et al., 2020; Wu et al., 2013), while in India, in several areas it varies from 7 to 23 $\mu\text{g m}^{-3}$ in different months (Singh et al., 2018). In the USA and European countries, BC concentrations are much smaller (<1–2 $\mu\text{g m}^{-3}$) and decreasing since 1960 (Herich et al., 2011; Kirchstetter et al., 2017).

The growth of AOD due to urban emissions in contrast to PM₁₀, is not very large and even the 3-fold increase (A3TU experiment) provides smaller AOD than that in the standard emission experiment with CAMS lateral boundary conditions (A1CTU experiment). On average, the urban AOD is about 0.029 (A1TU experiment, see Table 1), comprising 20–30% of the total AOD. The urban component of surface aerosol mass concentration is much higher: about 86% for BC and 74% for PM₁₀. This is in a qualitative agreement with our

previous assessments (Chubarova et al., 2022).

For testing urban AOD (ΔAOD), we used the difference between the estimates at the MSU MO and Zvenigorod. The mean model and observed ΔAOD are in an agreement: 0.019 ± 0.012 (0.0202 ± 0.011) according to the A1CTU(A1CU) experiments with standard emissions and 0.016 ± 0.013 – according to measurements. These values are slightly smaller than model urban AOD, shown in Table 1, since Zvenigorod may be also affected by Moscow urban plumes. The A3TU and A3CTU experiments with the 3-fold emissions provided larger ΔAOD of about 0.042 ± 0.03 and 0.041 ± 0.025 . Maximum ΔAOD was observed for the A3BTU experiment when $\Delta\text{AOD} = 0.046 \pm 0.023$. Fig. 2 demonstrates similar tendency in changes of the modeled and measured ΔAOD in clear sky conditions. However, one can see a large deviation, especially when the observed ΔAOD s are low. According to observation we also obtained 8 cases with negative ΔAOD depicting the situations with higher AOD in Zvenigorod, which were not reproduced by the model (not shown).

The urban canopy effects determined as the difference between the ctrl_TU and ctrl_T experiments, are expressed in the decrease of surface albedo on 2.2% from 19.1% to 16.9% with consideration of urban canopy: urban canyons, roofs, pavements with lower surface albedo (Wouters et al., 2016). The observed local surface grass albedo is about 20%, however, it characterizes only local conditions at the MSU MO without accounting for spatial urban heterogeneity. The lower surface albedo decreases the multiple reflection and affects diffuse irradiance as well as net radiation at BOA and TOA (see the analysis below).

3.1.2. Radiative effects in clear and all-sky conditions

Radiative aerosol effects were studied using different numerical experiments in clear sky and all-sky conditions. Fig. 3 presents mean changes in direct, diffuse, global irradiance, net shortwave (s/w) irradiance at BOA, net s/w irradiance at TOA and net longwave (l/w) irradiance at TOA in the cloudless atmosphere. The differences in the model experiments described in Table S3, provide evaluating the radiation sensitivity to different emissions, to the boundary CAMS conditions, Tegen climatology, and to the urban parameterization. The urban aerosol provides a distinct decrease in direct and corresponding increase in diffuse irradiance. The latter is smaller for highly absorbing aerosol (12 W m^{-2} and 5 W m^{-2} respectively). For global irradiance there is a pronounced decrease from about 5 W m^{-2} for standard emissions to 30 W m^{-2} for highly absorbing urban aerosol at 3-fold emissions.

The changes in net irradiance at TOA(BOA) for the ART, ART3, and ART3B30 experiments corresponds to the shortwave and longwave ERF. The urban AOD provides negative shortwave ERF from -0.9 to -3.4 W m^{-2} for weakly absorbing aerosol at TOA depending on emission rates (see Fig. 7e). On the contrary, the ERF for highly absorbing aerosol (ART3B30) is positive ($+2.5 \text{ W m}^{-2}$). The shortwave aerosol radiative effects in the ART+CAMSb, ART3 + CAMSb, ART+CAMSb_noT experiments provide negative ARE assessments of about $3\text{--}5 \text{ W m}^{-2}$ at TOA (see Fig. 3e) and $8\text{--}15 \text{ W m}^{-2}$ at BOA. The s/w ARE estimates with and without application of the Tegen climatology are similar.

Longwave irradiance does not undergo significant changes due to prevailing fine aerosol mode in Moscow and, hence, negligible radiative effects in the infrared spectral range. As a result, due to aerosol absorption longwave ERF at TOA is small and positive for standard and 3-fold emissions ($+0.1$, $+0.5 \text{ W m}^{-2}$, respectively), and to some extent compensates the s/w ERF.

The account of the urban canopy provides a decrease in diffuse irradiance due to more effective absorption at surface at lower surface albedo (see Table 1) as well as an increase in both net s/w irradiance at the TOA and BOA (see Fig. 3 d,e). The changes in l/w irradiance are negative (see Fig. 3 f) due to additional emitting of urban heat. However, they are significantly lower than corresponding

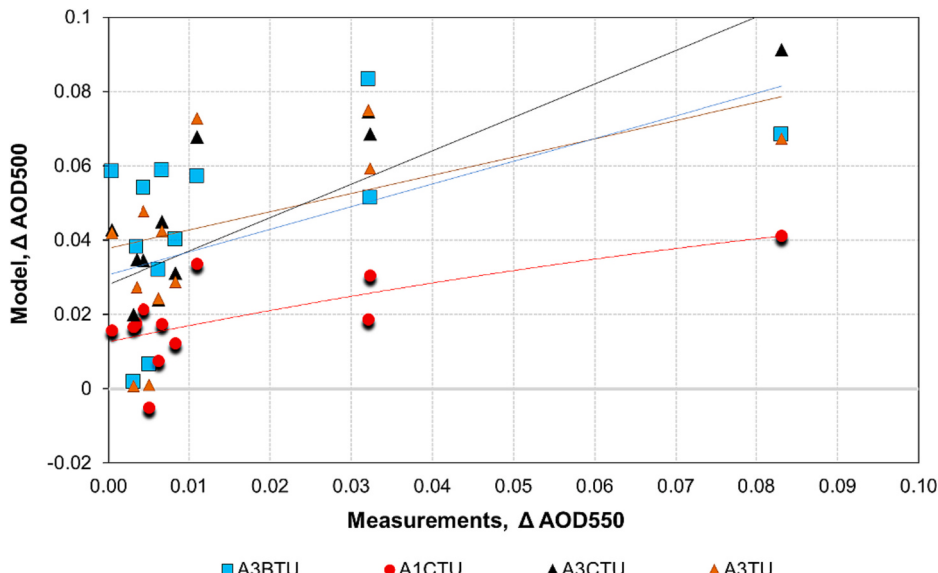


Fig. 2. The comparisons between the ΔAOD obtained from measurements and from different model experiments (see Table S2 for acronym descriptions). Clear sky conditions.

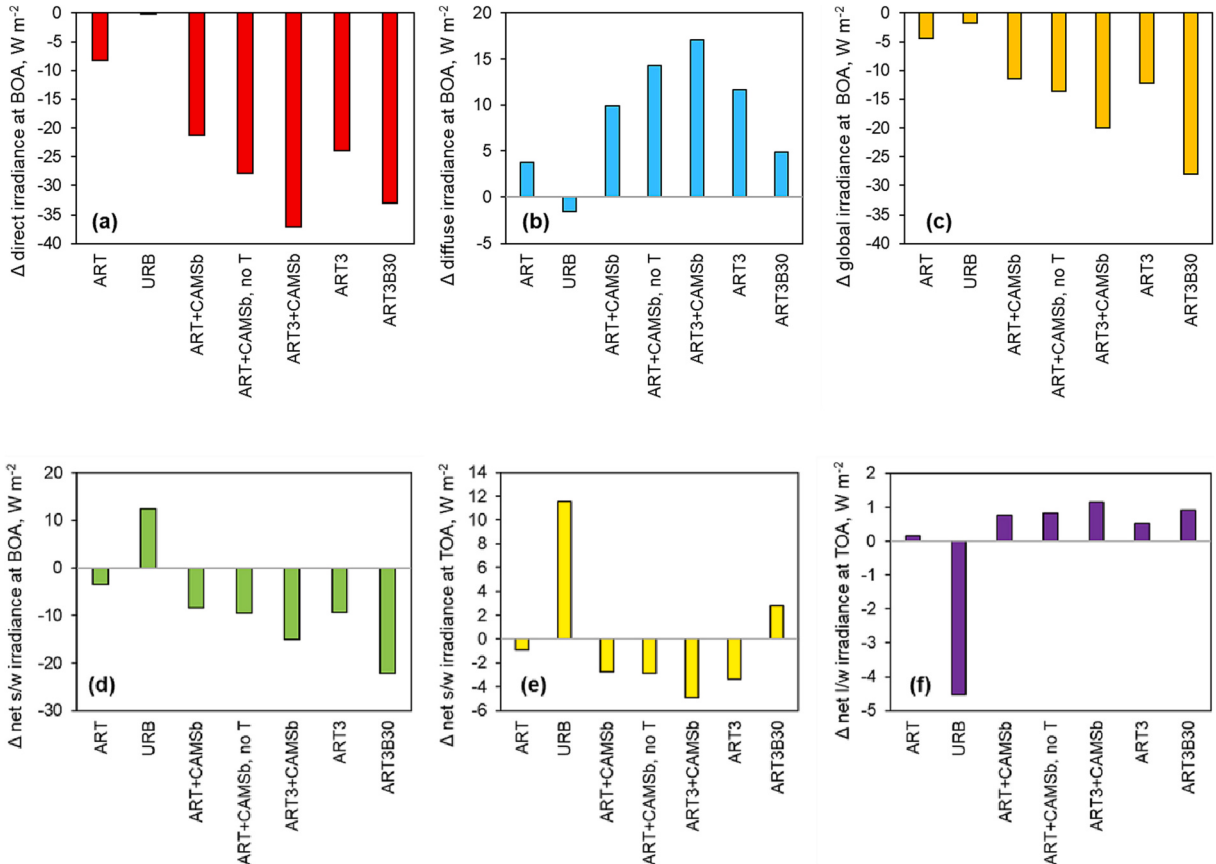


Fig. 3. Mean differences (Δ) in direct (a), diffuse (b), global (c) irradiance, net s/w irradiance at the bottom of the atmosphere (BOA) (d), net s/w irradiance at the top of the atmosphere (TOA) (e), and net l/w irradiance at TOA (f) for evaluating the effects of different model configurations and emissions. See Table S3 for the description of the experiments. Clear sky conditions. MSU MO.

changes in s/w net irradiance.

All-sky conditions combine both direct and semi-direct radiative effects of aerosol. Semi-direct aerosol effects influence temperature and relative humidity structure, which can affect cloud formation or its dissipation (Allen et al., 2019; Tsikerdeks et al., 2019). Table 2 summarizes the mean ERF and ARE estimates in clear and all-sky conditions for the experiment with standard emissions. Both in clear and all-sky conditions at TOA and BOA the s/w ERF and ARE values have negative signs and on average are in line with the estimates shown in IPCC (2014), however, in all-sky conditions they are not statistically significant due to large variations in the cloudy atmosphere. L/w ERF and ARE values are small positive in clear sky, but could be of different signs in all-sky conditions. As a result, total (s/w plus l/w) ERF and ARE estimates are negative, providing cooling of the atmosphere.

We also see some changes in cloudiness in all-sky conditions due to perturbation of temperature and humidity vertical profiles, which result in a small mean difference in total cloud amount, which varies from -0.03 to 0.01 and is not statistically significant, however, locally noticeable changes may occur (see maxima and minima Nt estimates in Table 2).

3.1.3. Aerosol effect on air temperature and its comparison with urban heat island

Fig. 4 shows temperature response to ERF and ARE at TOA for clear sky conditions due to the effects of weakly and highly absorbing aerosols. One can see negative changes in temperature, except some cases with small ERF, when other factors may play some role. However, for weakly absorbing aerosol we see positive changes in temperature with the increase in ERF at smaller AOD due to less scattering. For highly absorbing aerosol, on the contrary, the increase in positive ERF provides a pronounced decrease in temperature, since the most intensive absorption and heating takes place in the atmosphere and not at ground level.

As a result, both absorbing and non-absorbing aerosols to some extent compensate for the urban heat island effect, however, this compensation is not large. For MSU MO conditions the mean temperature increase due to TERRA.URB parameterization, i.e. UHI, is about 1.5°C during daytime, while the maximum negative temperature effects of aerosol reach 0.5°C for the 3-fold increase in urban emissions (ART3 + CAMSb). So even the maximum aerosol effects do not compensate for the temperature increase due to urban heat island.

We also examine the changes in total net irradiance at TOA, as well as cloud amount and temperature due to both direct and semi-direct effects in all-sky conditions. Fig. 5 presents the ARE and ERF estimates, as well as total net radiation changes due to URB effects

Table 2

The estimates of effective radiative forcing and aerosol radiative effects in clear sky (direct effects) and all-sky conditions (direct and semi-direct effects) at the top (TOA) and at the bottom of the atmosphere (BOA) for shortwave (s/w), longwave (l/w) and total irradiance (total) and their influence on total cloud amount Nt. Daytime conditions ($h_{\text{sun}} > 0$). MSU MO.

Statistics	Clear sky conditions						All-sky conditions								
	Effective radiative aerosol forcing, ERF (ART experiment)														
	BOA, s/w W m ⁻²	TOA s/w W m ⁻²	BOA l/w W m ⁻²	TOA l/w W m ⁻²	total BOA W m ⁻²	total TOA W m ⁻²	Nt	BOA s/w W m ⁻²	TOA s/w W m ⁻²	BOA l/w W m ⁻²	TOA l/w W m ⁻²	BOA total W m ⁻²	TOA total W m ⁻²	Nt	
10	mean	-3.4	-0.9	0.3	0.1	-3.1	-0.7	0	-4.5	-1.5	0.0	-0.2	-4.4	-1.7	-0.03
	sigma	2.2	0.8	0.4	0.2	2.0	0.7	0	19.1	18.4	5.6	4.3	17.0	16.7	0.87
	max	-0.4	0.4	1.1	0.5	-0.1	0.5	0	67.5	70.9	30.8	15.8	63.2	67.4	4.43
	min	-8.7	-2.6	-0.8	-0.2	-7.8	-2.2	0	-156.3	-142.2	-21.2	-24.8	-151.6	-139.1	-5.55
Aerosol Radiative effect, ARE (ART + CAMSb experiment)															
	mean	-8.5	-2.7	1.2	0.8	-7.3	-2.0	0	-8.5	-1.9	1.1	0.4	-7.4	-1.6	0.01
	sigma	4.2	1.4	0.7	0.4	3.7	1.2	0	38.2	36.7	11.5	9.0	31.5	32.2	1.53
	max	-0.9	0.1	2.7	1.6	0.2	0.8	0	291.8	281.1	33.4	32.9	244.1	262.8	8.50
	min	-16.8	-5.2	0.2	0.1	-14.1	-3.7	0	-158.0	-154.9	-73.2	-61.8	-134.2	-136.7	-9.03

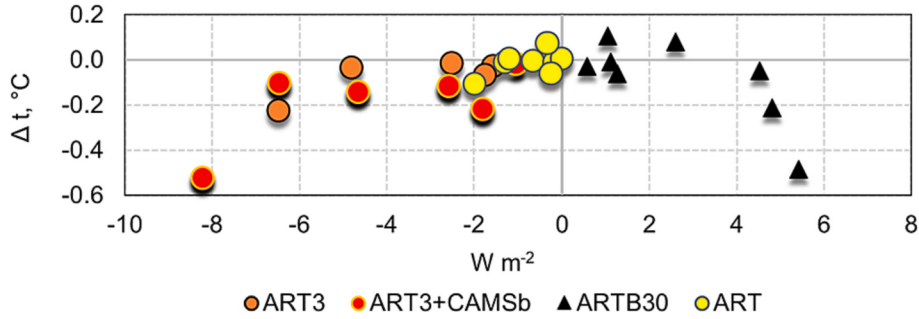


Fig. 4. Changes of temperature at 2 m (Δt , $^{\circ}\text{C}$) as a function of aerosol s/w ERF obtained from different model experiments with weakly absorbing urban aerosols at different level of emissions (ART, ART3), highly absorbing aerosol (ARTB30), and aerosol radiative effect (ART3 + CAMSb) in clear sky conditions.

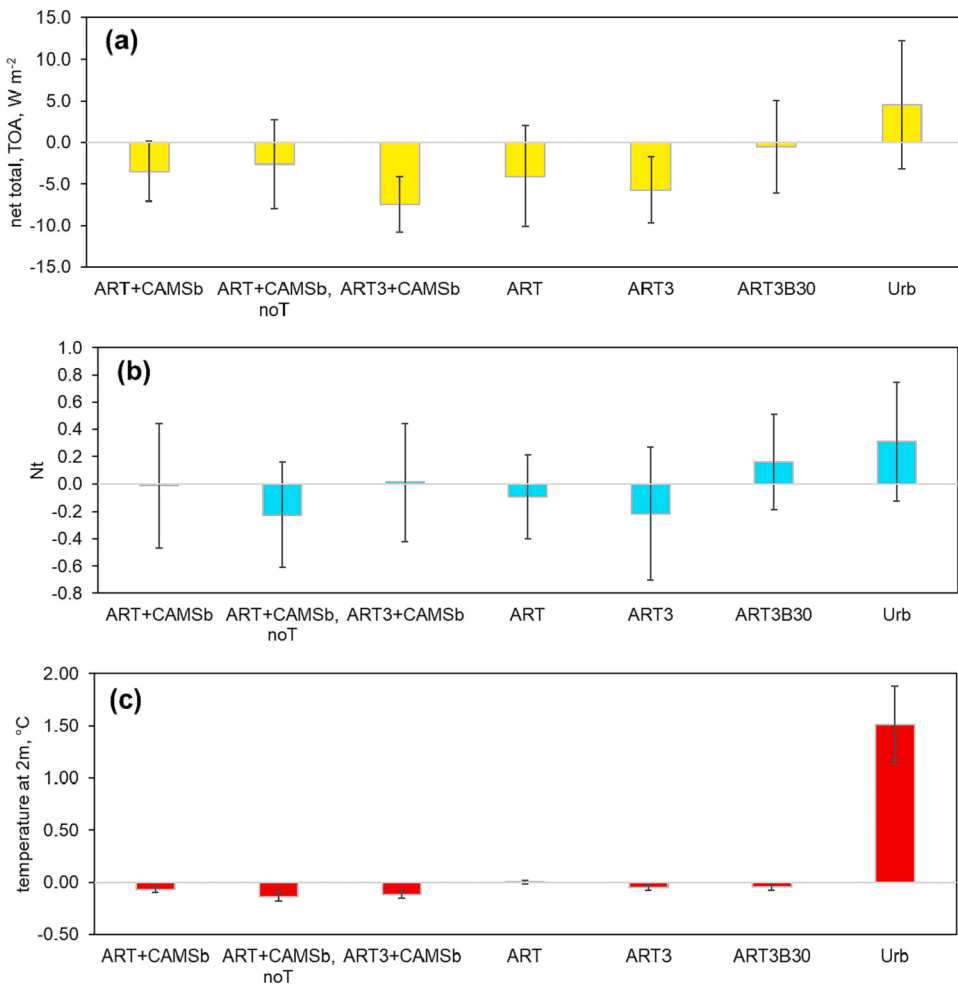


Fig. 5. Mean response in total (s/w plus l/w) net irradiance at TOA (a), in total cloud amount N_t (b), and in temperature at 2 m, $^{\circ}\text{C}$ (c) to different model configurations and emissions in all-sky conditions. See Table S3 for the description of the experiments. MSU MO. Daytime conditions.

at TOA, and corresponding cloud amount changes and temperature at 2 m. One can see that in all experiments aerosol-induced radiative changes are negative compared to the positive urban effect. The latter, however, is not statistically significant. We also see a tendency of cloud amount decreasing in conditions of weakly absorbing aerosol and its increasing in highly absorbing aerosol conditions as well as in the case of the urban canopy account. However, all the changes are not statistically significant possibly due to relatively small statistics and strong variation of clouds. Similar to clear sky conditions, there is no compensation of the UHI by urban

aerosol even with 3-fold emissions, when mean aerosol-induced temperature effects reach -0.13°C compared to the UHI of $+1.5^{\circ}\text{C}$.

3.2. Spatial distribution of aerosol and its radiative and temperature effects over Moscow

According to different numerical experiments we analyzed spatial distribution of PM₁₀ and radiative and temperature effects due to different columnar aerosol properties. Fig. 6 presents an example of the model PM₁₀ spatial distribution on May 1st, 2019 together with the observed PM₁₀ concentrations at the Mosecomonitoring sites. The upper panel shows the PM₁₀ distribution using standard emissions with and without CAMS boundary conditions and Tegen climatology, while in the low panel PM₁₀ concentration has been generated using the 3-fold emission rates with different aerosol properties. One can see close results between the experiments with similar levels of emissions. The comparisons with the observations at different sites show that in some cases PM₁₀ concentrations are in a better agreement with simulations at standard emissions and in some - at the 3-fold emissions. For studying this effect, we made comparisons between the observed and model PM₁₀ for the sites combined together according to their classification depending on distance from the pollution source.

The results are presented in Fig. 7, where the model and measured mean PM₁₀ concentrations over the natural areas, residential areas, the areas close to mixed pollution sources, and the areas close to highways are shown. In addition, we show mean road area fraction in corresponding cells. It is interesting that the mean road area fraction is lower at the sites located close to mixed pollution sources than that in residential areas. This provides quite similar observed PM₁₀ concentration there (about $34 \mu\text{g m}^{-3}$). This could happen, since this classification has been developed about 20 years ago, and due to recent active Moscow development, several sites in the residential areas and in the areas with the mixed pollution sources could change their characteristics. However, if we compare the observed PM₁₀ concentrations at the clean sites over natural areas located in city background conditions in the proximity of green zones and at the sites, close to highways we found a noticeable PM₁₀ increase (from $26 \mu\text{g m}^{-3}$ to $48 \mu\text{g m}^{-3}$). For natural areas there is a reasonable agreement ($26 \mu\text{g m}^{-3}$ and $24 \mu\text{g m}^{-3}$) between PM₁₀ modeling with standard emissions and the account of CAMS boundary conditions (A1CTU, A1CU experiments), while the 3-fold emissions provide too high concentrations. At the sites located close to highways we see an increase in model PM₁₀ concentrations up to $29 \mu\text{g m}^{-3}$ at standard emission rate, however, this is much lower than the observed values. The 3-fold emissions, on the contrary, provides too high concentrations (larger than $70 \mu\text{g m}^{-3}$). So, in model simulations we have a right tendency of increasing the PM₁₀ concentrations from clean sites to highly polluted ones, but this increase is quite small (17–31%), while the increase obtained from observations is characterized by 82% growth (see Fig. 7). This may happen due to the effects of the application of a 2 km space grid, which may provide significant smoothing and, as a result, lower PM₁₀ concentration compared to the local measurements, especially over highly polluted areas. Srimath et al. (2017) also showed similar underestimation of PM₁₀ in London and Birmingham near highways. The noticeable discrepancy between measured and modeled PM₁₀ were also mentioned in Berlin and Paris (Beekmann et al., 2007; Royer et al., 2011). For a better description of the effects of local emission sources, neural networks may be used (Shepelev et al., 2023). We plan to study these processes in more detail in the future.

Using model aerosol properties, we estimated aerosol shortwave and longwave effective radiative forcing ERF at the top and at the

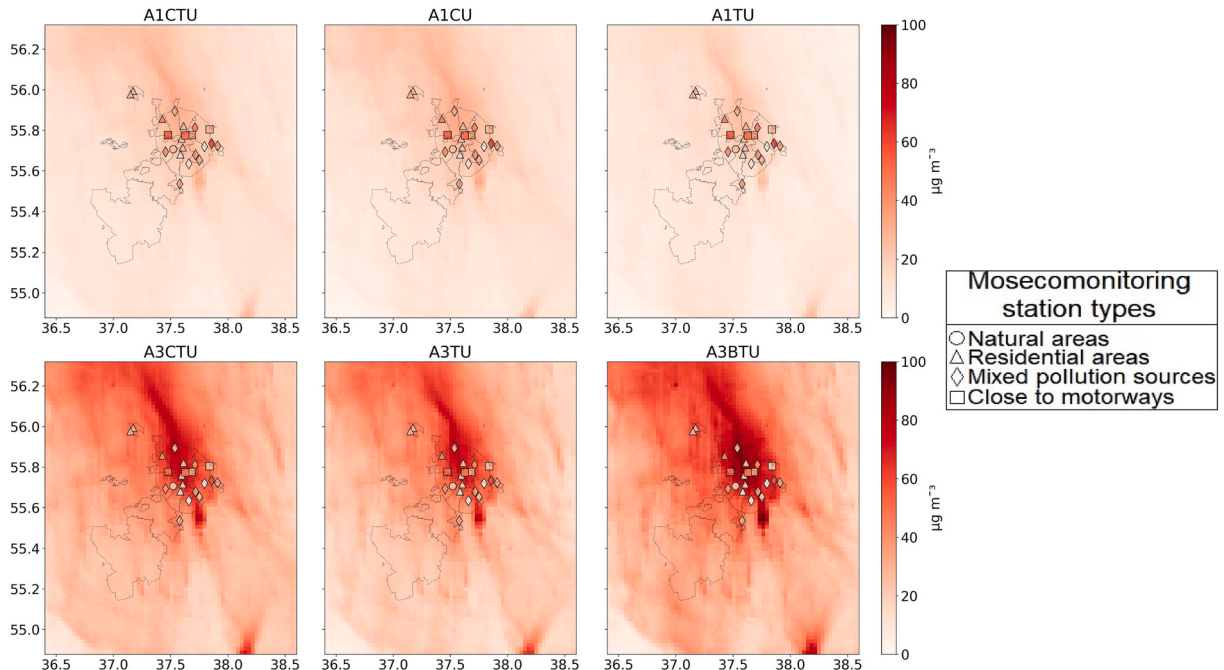


Fig. 6. An example of PM₁₀ distribution over Moscow region obtained from different numerical experiments (see Table S2) and the results of observations at different Mosecomonitoring sites (shown by circles). 01.05.2019. 9 h Local Time.

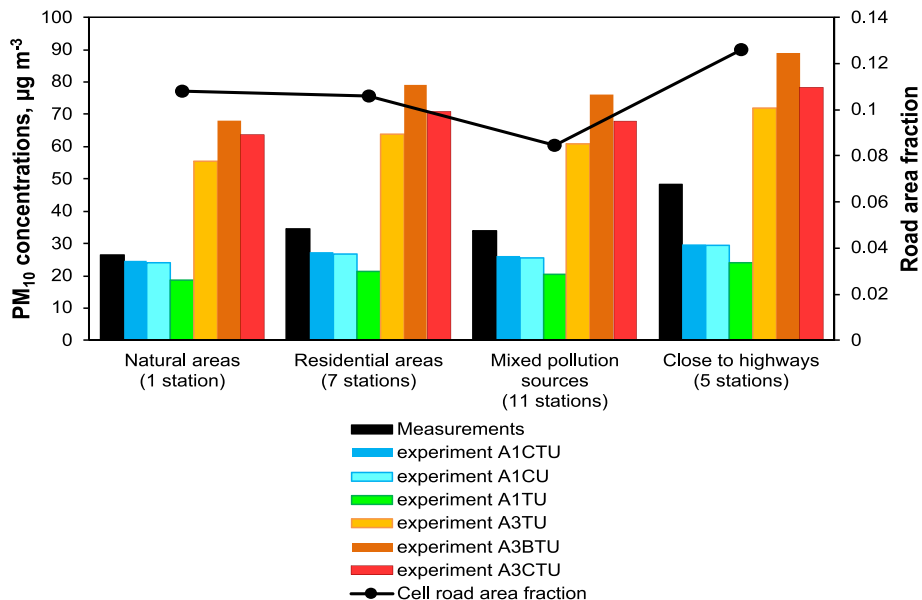


Fig. 7. The distribution of model and measured mean PM_{10} concentrations at four types of Mosecomonitoring sites and the mean road area fraction in corresponding cells.

bottom of the atmosphere. Fig. 8 presents an example of its distribution in clear sky conditions over the Moscow region for a similar date and time as shown for PM_{10} in Fig. 6. There is a pronounced negative shortwave ERF over the central part of Moscow city up to -3 W m^{-2} at TOA and up to -9 W m^{-2} at surface. Longwave ERF is positive due to the effects of aerosol absorption, however, it is much smaller than shortwave ERF due to prevailing fine aerosol mode. As a result, the total ERF (not shown) follows the changes in shortwave ERF. Wind direction shown in Fig. 8 by arrows explains the configuration of the polluted PM_{10} plume distributed approximately from south to north over the Moscow region for this particular case.

To summarize radiative and temperature feedbacks over the whole territory of Moscow region we made the composite maps of AOD, radiative and temperature effects. In addition, we simulated the radiative atmospheric absorption response A due to urban aerosols using the following equation:

$$A = [N_{TOA}(\text{AITU}) - N_{BOA}(\text{AITU})] - [N_{TOA}(\text{ctrl_TU}) - N_{BOA}(\text{ctrl_TU})], \quad (4)$$

where N is the net irradiance at TOA and BOA, estimated in the experiment with the standard urban emission (A1TU) and in the experiment without urban emissions (ctrl_TU).

Fig. 9 presents the AOD, atmospheric absorption response and the changes in air temperature at 2 m for clear and all-sky conditions for the experiment with standard urban emissions (ART experiment according to Table S3). For clear sky conditions one can see a localization of AOD over central Moscow area as well as an increase in atmospheric radiative absorption of up to 4 W m^{-2} . This should provide heating of the atmosphere over Moscow's central area and influence on the temperature gradient, which may affect the atmosphere dynamics. However, at ground level the changes in temperature are almost always negative and very small.

In all-sky conditions at standard emissions the AOD spatial distribution is also localized over the central Moscow area providing a pronounced increase in atmospheric absorption up to 5 W m^{-2} . However, the relatively small mean surface temperature effects (up to -0.15°C) were biased to the north due to a small positive change in cloud amount, possibly, because of semi-direct effects over this area.

4. Conclusions

Using the COSMO-ART model with 2 km grid spacing, we estimated aerosol properties and their radiative and temperature effects in Moscow megacity. The magnitude of the aerosol anthropogenic impact on atmospheric radiation and temperature was estimated using numerical simulations with different emission levels. By setting 3-fold emissions, we estimated the upper urban aerosol pollution with weakly and highly absorbing aerosol. Aerosol effects were compared with the urban canopy effects including UHI, which have been estimated according to simulations with and without the account of TERRA_URB parameterization.

The mean urban aerosol optical depth was about 0.029, comprising 20–30% of the total AOD, which is in agreement with the observations. For a relatively clean MSU MO site we showed a satisfactory agreement between measured and model PM_{10} concentrations at standard emission rates. Urban components of PM_{10} and BC at surface were 74% and 86% of their total content.

Depending on emission rates, the urban AOD provided negative shortwave ERF of about $0.9\text{--}3.4 \text{ W m}^{-2}$ for weakly absorbing aerosol at TOA, while ERF estimates for highly absorbing aerosol, on the contrary, were positive (up to $+2.5 \text{ W m}^{-2}$). The application

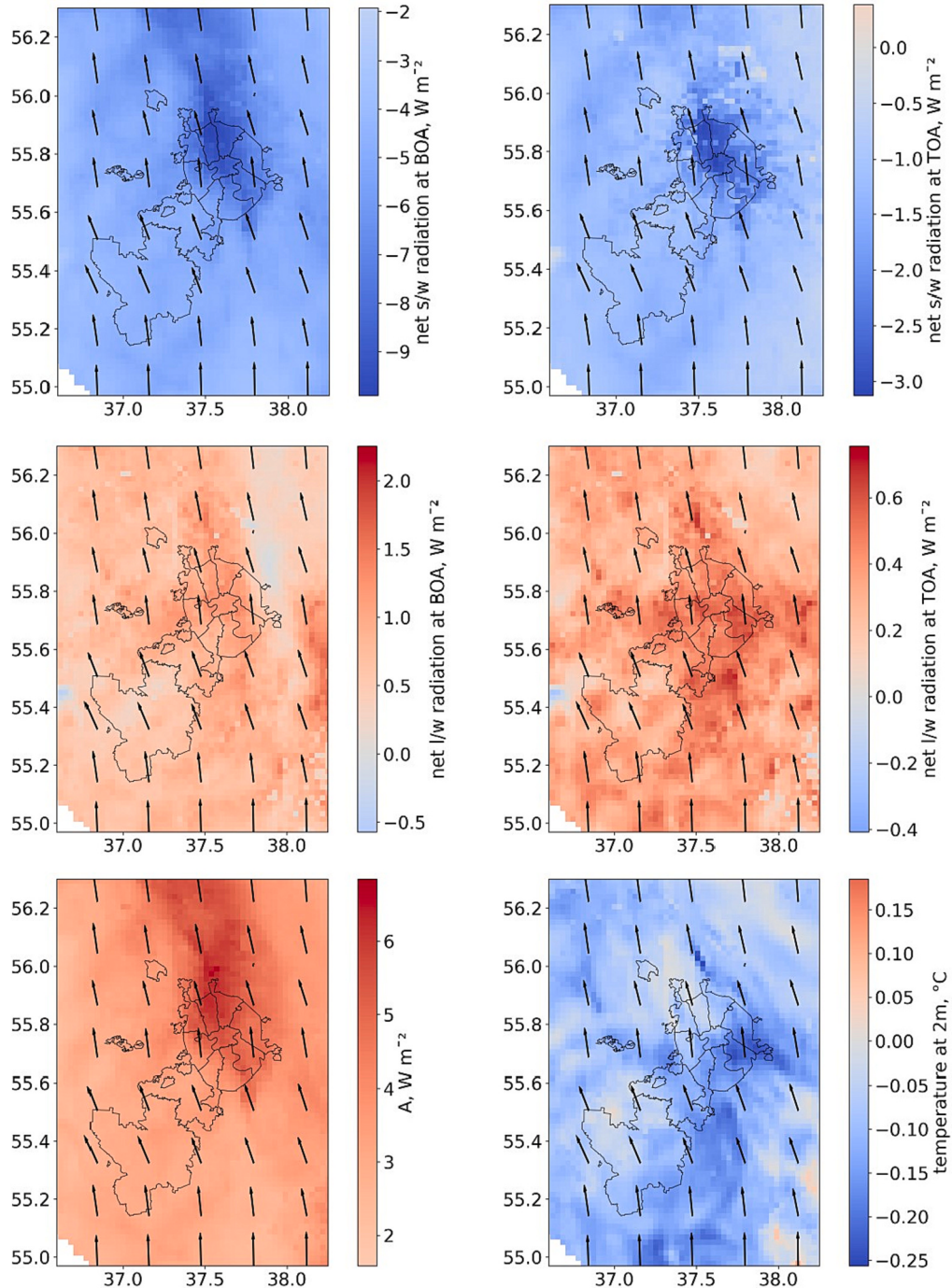


Fig. 8. The ERF assessment according to the ART experiment (see Table S3 for the details) for s/w (upper panel), l/w (middle panel) net irradiance at BOA (left column) and at TOA (right column). In the low panel urban AOD and response in temperature at 2 m are presented. 01.05.2019. 9 h Local Time. Clear sky conditions. Wind direction is shown by arrows.

of the TERRA_URB parameterization led to the decrease in surface albedo from 19.1% to 16.9%, which resulted in positive shortwave ERF, while negative longwave ERF was observed due to additional emitting of urban heat.

The air temperature at 2 m decreased with the increase of both weakly and highly absorbing aerosols at different emission rates without the dependence on the sign of the ERF. This aerosol-induced cooling partially compensated for the UHI during daytime: the temperature decrease due to aerosol reached 0.5 °C at the 3-fold increase in urban emissions, while the UHI effect was 1.5 °C.

The composite maps for clear sky conditions have revealed a localization of urban AOD over the central city area providing an

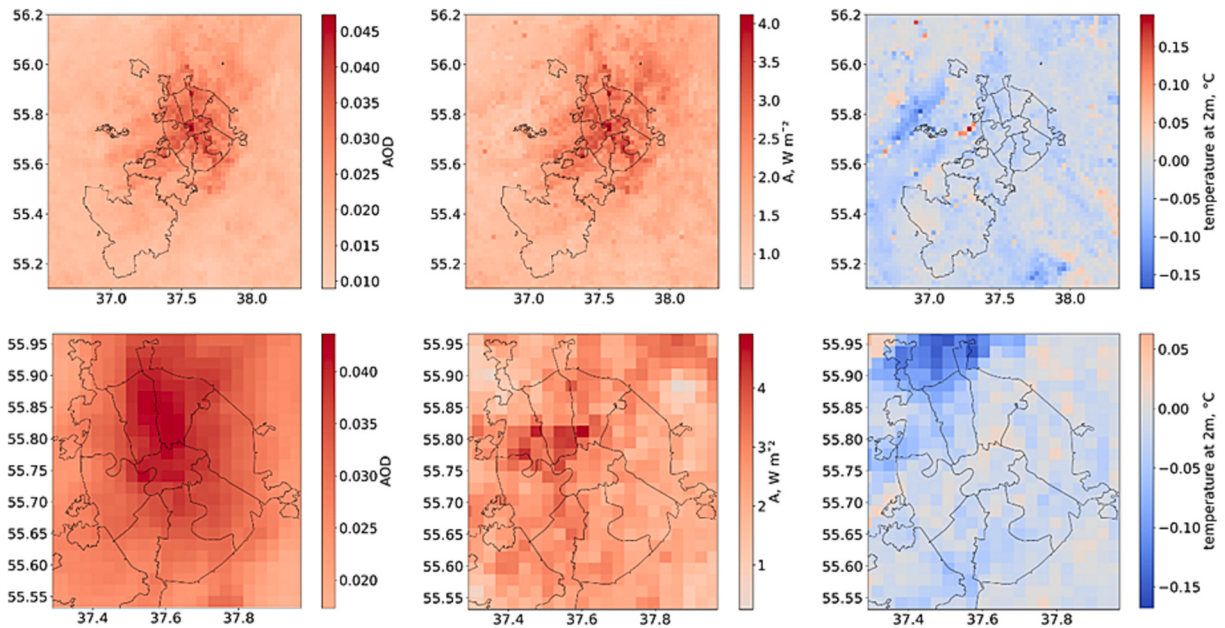


Fig. 9. The composites of urban AOD (left column), atmospheric absorption response $A, \text{W m}^{-2}$ (middle column) and temperature effect at 2 m, $^{\circ}\text{C}$ (right column) due to the ART experiment over the whole period of observations from 6 am to 6 pm for clear sky (upper panel) and all-sky (low panel) conditions. The description of the ART experiment is given in Table S3.

increase in the atmospheric radiative absorption up to 4 W m^{-2} . This should lead to additional heating of the low troposphere, affecting temperature profile and atmospheric dynamics. At surface the changes in temperature due to aerosol were negative and small. In all-sky conditions, mean temperature response significantly varied over Moscow with the maximum mean negative temperature of $-0.15 ^{\circ}\text{C}$.

In the future, we are planning to perform additional model experiments, which will cover large period and contrast meteorological conditions with different surface albedo and temperature regime.

Funding

The bulk of work was supported by the Ministry of Education and Science of the Russian Federation, megagrant no. 075-15-2021-574. This research was performed according to the Development Program of the MSU Interdisciplinary Scientific and Educational School “Future Planet and Global Environmental Change” at the Lomonosov Moscow State University. Supercomputer simulations were supported by the Federal Service for Hydrometeorology and Environmental Monitoring of Russia (topic no. AAAA-A20-120021490079-3). The work on setting up the COSMO-ART model with TERRA_URB parameterization for Moscow region performed by M. Varentsov and A. Kirsanov was partially supported by Russian Science Foundation, project no. 23-77-30008.

CRediT authorship contribution statement

Natalia Chubarova: Conceptualization, Methodology, Supervision, Investigation, Writing – original draft, Writing – review & editing. **Elizaveta Androsova:** Data curation, Visualization, Validation, Investigation, Formal analysis. **Alexander Kirsanov:** Software, Visualization, Investigation, Validation, Methodology, Data curation, Formal analysis, Writing – original draft. **Mikhail Varentsov:** Software, Conceptualization, Visualization, Investigation, Validation, Methodology, Writing – original draft. **Gdalyiv Rivin:** Methodology, Software.

Declaration of Competing Interest

The authors declare that they have no known competing financial interests or personal relationships that could have appeared to influence the work reported in this paper.

Data availability

The datasets used or analyzed during the current study are available from the corresponding author on request.

Acknowledgements

We are grateful to Dr. Alexander Makhura and Dr. Pauli Paasonen for fruitful discussions, as well as to the staff of the IAP RAS for providing AERONET data at the Zvenigorod site. In addition, we would like to thank two anonymous reviewers for valuable comments.

Appendix A. Supplementary data

Supplementary data to this article can be found online at <https://doi.org/10.1016/j.uclim.2023.101762>.

References

- Allen, R.J., Amiri-Farahani, A., Lamarque, J.-F., Smith, C., Shindell, D., Hassan, T., Chung, C.E., 2019. Observationally constrained aerosol–cloud semi-direct effects. *NPJ Clim. Atmos. Sci.* 2, 16. <https://doi.org/10.1038/s41612-019-0073-9>.
- Baldauf, M., Seifert, A., Förstner, J., Majewski, D., Raschendorfer, M., Reinhardt, T., 2011. Operational convective-scale numerical weather prediction with the COSMO model: description and sensitivities. *Mon. Weather Rev.* 139, 3887–3905. <https://doi.org/10.1175/MWR-D-10-05013.1>.
- Beckmann, M., Kerschbaumer, A., Reimer, E., Stern, R., Möller, D., 2007. PM measurement campaign HOVERT in the greater Berlin area: model evaluation with chemically specified particulate matter observations for a one year period. *Atmos. Chem. Phys.* 7, 55–68. <https://doi.org/10.5194/acp-7-55-2007>.
- Bond, T.C., Doherty, S.J., Fahey, D.W., Forster, P.M., Berntsen, T., DeAngelo, B.J., Flanner, M.G., Ghan, S., Kärcher, B., Koch, D., Kinne, S., Kondo, Y., Quinn, P.K., Sarofim, M.C., Schultz, M.G., Schulz, M., Venkataraman, C., Zhang, H., Zhang, S., Bellouin, N., Guttikunda, S.K., Hopke, P.K., Jacobson, M.Z., Kaiser, J.W., Klimont, Z., Lohmann, U., Schwarz, J.P., Shindell, D., Storelvmo, T., Warren, S.G., Zender, C.S., 2013. Bounding the role of black carbon in the climate system: a scientific assessment. *J. Geophys. Res. Atmos.* 118, 5380–5552. <https://doi.org/10.1002/jgrd.50171>.
- Buchhorn, M., Lesiv, M., Tsendbazar, N.-E., Herold, M., Bertels, L., Smets, B., 2020. Copernicus global land cover layers—collection 2. *Remote Sens.* 12, 1044. <https://doi.org/10.3390/rs12061044>.
- Cao, C., Lee, X., Liu, S., Schultz, N., Xiao, W., Zhang, M., Zhao, L., 2016. Urban heat islands in China enhanced by haze pollution. *Nat. Commun.* 7, 12509. <https://doi.org/10.1038/ncomms12509>.
- Carey, I.M., Anderson, H.R., Atkinson, R.W., Beavers, S., Cook, D.G., Dajnak, D., Gulliver, J., Kelly, F.J., 2016. Traffic pollution and the incidence of cardiorespiratory outcomes in an adult cohort in London. *Occup. Environ. Med.* <https://doi.org/10.1136/oemed-2015-103531> oemed-2015-103531.
- Chou, M., Lin, P., Ma, P., Lin, H., 2006. Effects of aerosols on the surface solar radiation in a tropical urban area. *J. Geophys. Res. Atmos.* 111 <https://doi.org/10.1029/2005JD006910>.
- Chubarova, N., Smirnov, A., Holben, B., 2011a. Aerosol properties in Moscow according to 10 years of AERONET measurements at the meteorological Observatory of Moscow State University. *Geogr. Environ. Sustain.* 4, 19–32. <https://doi.org/10.24057/2071-9388-2011-4-1-19-32>.
- Chubarova, N.Y., Sviridenkov, M.A., Smirnov, A., Holben, B.N., 2011b. Assessments of urban aerosol pollution in Moscow and its radiative effects. *Atmos. Meas. Tech.* 4, 367–378. <https://doi.org/10.5194/amt-4-367-2011>.
- Chubarova, N., Zhdanova, Y., Androsova, Y., Kirsanov, A., Shatunova, M., Khlestova, Y., Volpert, Y., Poliukhov, A., Eremina, I., Vlasov, D., Popovicheva, O., Ivanov, A., Gorbarenko, Y., Nezval, Y., Blinov, D., Rivin, G., 2020. The aerosols urban pollution and its effects on weather, regional climate and geochemical processes. LLC MAKS Press. <https://doi.org/10.29003/m1475.978-5-317-06464-8>.
- Chubarova, N.E., Vogel, H., Androsova, A.A., Kirsanov, A.B., Vogel, B., Rivin, G.S., 2022. Columnar and surface urban aerosol in the Moscow megacity according to measurements and simulations with the COSMO-ART model. *Atmos. Chem. Phys.* 22, 10443–10466. <https://doi.org/10.5194/acp-22-10443-2022>.
- Crutzen, P., 2004. New directions: the growing urban heat and pollution “island” effect—impact on chemistry and climate. *Atmos. Environ.* 38, 3539–3540. <https://doi.org/10.1016/j.atmosenv.2004.03.032>.
- Dinkelacker, B., 2023. Chemical transport modeling of atmospheric aerosol at regional and urban scales. <https://doi.org/10.1184/R1/22029092.v1>.
- Duarte, R.M.B.O., Duarte, A.C., 2020. Urban atmospheric aerosols: sources, analysis, and effects. *Atmosphere* 11, 1221. <https://doi.org/10.3390/atmos1111221>.
- Dubovik, O., King, M.D., 2000. A flexible inversion algorithm for retrieval of aerosol optical properties from Sun and sky radiance measurements. *J. Geophys. Res. Atmos.* 105, 20673–20696. <https://doi.org/10.1029/2000JD900282>.
- Folberth, G.A., Rumbold, S.T., Collins, W.J., Butler, T.M., 2012. Global radiative forcing and megacities. *Urban Clim.* 1, 4–19. <https://doi.org/10.1016/j.uclim.2012.08.001>.
- Garbero, V., Milelli, M., Buccignani, E., Mercogliano, P., Varentsov, M., Rozinkina, I., Rivin, G., Blinov, D., Wouters, H., Schulz, J.-P., Schättler, U., Bassani, F., Demuzere, M., Repola, F., 2021. Evaluating the urban canopy scheme TERRA_URB in the COSMO model for selected European cities. *Atmosphere* 12, 237. <https://doi.org/10.3390/atmos12020237>.
- Giles, D.M., Sinyuk, A., Sorokin, M.G., Schafer, J.S., Smirnov, A., Slutsker, I., Eck, T.F., Holben, B.N., Lewis, J.R., Campbell, J.R., Welton, E.J., Korkin, S.V., Lyapustin, A.I., 2019. Advancements in the Aerosol Robotic Network (AERONET) Version 3 database – automated near-real-time quality control algorithm with improved cloud screening for Sun photometer aerosol optical depth (AOD) measurements. *Atmos. Meas. Tech.* 12, 169–209. <https://doi.org/10.5194/amt-12-169-2019>.
- Gliß, J., Mortier, A., Schulz, M., Andrews, E., Balkanski, Y., Bauer, S.E., Benedictow, A.M.K., Bian, H., Checa-Garcia, R., Chin, M., Ginoux, P., Griesfeller, J.J., Heckel, A., Kipling, Z., Kirkevåg, A., Kokkola, H., Laj, P., Le Sager, P., Lund, M.T., Lund Myhre, C., Matsui, H., Myhre, G., Neubauer, D., van Noije, T., North, P., Olivíe, D.J.L., Rémy, S., Sogacheva, L., Takemura, T., Tsigaridis, K., Tyro, S.G., 2021. AeroCom phase III multi-model evaluation of the aerosol life cycle and optical properties using ground- and space-based remote sensing as well as surface in situ observations. *Atmos. Chem. Phys.* 21, 87–128. <https://doi.org/10.5194/acp-21-87-2021>.
- Giusti, M., 2022. CAMS Reanalysis [WWW Document]. ECMWF. URL <https://www.ecmwf.int/en/research/climate-reanalysis/cams-reanalysis> (accessed 5.11.23).
- Granié, C., Damas, S., Lioussse, C., Middleton, P., Mieville, A., Paulin, M., Pignot, V., 2012. The ECCAD Database: Emissions of Atmospheric Compounds & Compilation of Ancillary Data. *IGAC Newsletter*, pp. 18–20.
- Herich, H., Hueglin, C., Buchmann, B., 2011. A 2.5 year’s source apportionment study of black carbon from wood burning and fossil fuel combustion at urban and rural sites in Switzerland. *Atmos. Meas. Tech.* 4, 1409–1420. <https://doi.org/10.5194/amt-4-1409-2011>.
- Hersbach, H., Bell, B., Berrisford, P., Hirahara, S., Horányi, A., Muñoz-Sabater, J., Nicolas, J., Peubey, C., Radu, R., Schepers, D., Simmons, A., Soci, C., Abdalla, S., Abellan, X., Balsamo, G., Bechtold, P., Biavati, G., Bidlot, J., Bonavita, M., De Chiara, G., Dahlgren, P., Dee, D., Diamantakis, M., Dragani, R., Flemming, J., Forbes, R., Fuentes, M., Geer, A., Haimberger, L., Healy, S., Hogan, R.J., Hölm, E., Janisková, M., Keeley, S., Laloyaux, P., Lopez, P., Lupu, C., Radnoti, G., de Rosnay, P., Rozum, I., Vamborg, F., Villaume, S., Thépaut, J., 2020. The ERA5 global reanalysis. *Q. J. R. Meteorol. Soc.* 146, 1999–2049. <https://doi.org/10.1002/qj.3803>.
- Holben, B.N., Eck, T.F., Slutsker, I., Tanré, D., Buis, J.P., Setzer, A., Vermote, E., Reagan, J.A., Kaufman, Y.J., Nakajima, T., Lavenu, F., Jankowiak, I., Smirnov, A., 1998. AERONET—A federated instrument network and data archive for aerosol characterization. *Remote Sens. Environ.* 66, 1–16. [https://doi.org/10.1016/S0034-4257\(98\)00031-5](https://doi.org/10.1016/S0034-4257(98)00031-5).

- Huang, Y., Zhang, Liuyi, Qiu, Y., Chen, Y., Shi, G., Li, T., Zhang, Lei, Yang, F., 2020. Five-year record of black carbon concentrations in urban Wanzhou, Sichuan Basin, China. *Aerosol Air Qual. Res.* 20, 1282–1293. <https://doi.org/10.4209/aaqr.2019.10.0516>.
- Inness, A., Ades, M., Agusti-Panareda, A., Barré, J., Benedictow, A., Blechschmidt, A.-M., Dominguez, J.J., Engelen, R., Eskes, H., Flemming, J., Huijnen, V., Jones, L., Kipling, Z., Massart, S., Parrington, M., Peuch, V.-H., Razinger, M., Remy, S., Schulz, M., Suttie, M., 2019. The CAMS reanalysis of atmospheric composition. *Atmos. Chem. Phys.* 19, 3515–3556. <https://doi.org/10.5194/acp-19-3515-2019>.
- IPCC, 2014. Climate Change 2013 – The Physical Science Basis. Cambridge University Press. <https://doi.org/10.1017/CBO9781107415324>.
- IPCC, 2023. Climate Change 2021 – The Physical Science Basis. Cambridge University Press. <https://doi.org/10.1017/9781009157896>.
- Jacobson, M.Z., 1998. Studying the effects of aerosols on vertical photolysis rate coefficient and temperature profiles over an urban airshed. *J. Geophys. Res. Atmos.* 103, 10593–10604. <https://doi.org/10.1029/98JD00287>.
- Jin, Q., Pryor, S.C., 2020. Long-term trends of high aerosol pollution events and their climatic impacts in North America using multiple satellite retrievals and modern-era retrospective analysis for research and applications version 2. *J. Geophys. Res. Atmos.* 125 <https://doi.org/10.1029/2019JD031137>.
- Jin, M., Shepherd, J.M., Zheng, W., 2010. Urban surface temperature reduction via the urban aerosol direct effect: a remote sensing and WRF model sensitivity study. *Adv. Meteorol.* 1–14. <https://doi.org/10.1155/2010/681587>.
- Jin, S., Ma, Y., Huang, Z., Huang, J., Gong, W., Liu, B., Wang, W., Fan, R., Li, H., 2023. A comprehensive reappraisal of long-term aerosol characteristics, trends, and variability in Asia. *Atmos. Chem. Phys.* 23, 8187–8210. <https://doi.org/10.5194/acp-23-8187-2023>.
- Kirchstetter, T.W., Preble, C.V., Hadley, O.L., Bond, T.C., Apte, J.S., 2017. Large reductions in urban black carbon concentrations in the United States between 1965 and 2000. *Atmos. Environ.* 151, 17–23. <https://doi.org/10.1016/j.atmosenv.2016.11.001>.
- Kirsanov, A., Rozinkina, I., Rivin, G., Zakharchenko, D., Olchev, A., 2020. Effect of natural forest fires on regional weather conditions in Siberia. *Atmosphere* 11, 1133. <https://doi.org/10.3390/atmos11101133>.
- Kuenen, J.J.P., Visschedijk, A.J.H., Jozwicka, M., Denier van der Gon, H.A.C., 2014. TNO-MACC II emission inventory; a multi-year (2003–2009) consistent high-resolution European emission inventory for air quality modelling. *Atmos. Chem. Phys.* 14, 10963–10976. <https://doi.org/10.5194/acp-14-10963-2014>.
- Kuenen, J., Dellaert, S., Visschedijk, A., Jalkanen, J.-P., Super, I., Denier van der Gon, H., 2022. CAMS-REG-v4: a state-of-the-art high-resolution European emission inventory for air quality modelling. *Earth Syst. Sci. Data* 14, 491–515. <https://doi.org/10.5194/essd-14-491-2022>.
- Kulbachevsky, A.O., 2022. Report on the state of the environment in Moscow in 2021 [WWW Document]. URL: <https://www.mos.ru/eco/documents/doklady/view/271573220/> (accessed 13.5.23).
- Kuznetsova, I.N., Rivin, G.S., Borisov, D.V., Shalygina, I.Yu., Kirsanov, A.A., Nakhaev, M.I., 2022. Modeling surface air pollution with reduced emissions during the COVID-19 pandemic using CHIMERE and COSMO-ART chemical transport models. *Russ. Meteorol. Hydrol.* 47, 174–182. <https://doi.org/10.3103/S106837922030025>.
- Liou, K.-N., 2010. *An Introduction to Atmospheric Radiation*. Int. geophysics series., 2nd ed. Academic Press.
- Liu, S., Xing, J., Zhao, B., Wang, J., Wang, S., Zhang, X., Ding, A., 2019. Understanding of aerosol-climate interactions in China: aerosol impacts on solar radiation, temperature, cloud, and precipitation and its changes under future climate and emission scenarios. *Curr. Pollut. Rep.* 5, 36–51. <https://doi.org/10.1007/s40726-019-00107-6>.
- Lu, F., Xu, D., Cheng, Y., Dong, S., Guo, C., Jiang, X., Zheng, X., 2015. Systematic review and meta-analysis of the adverse health effects of ambient PM2.5 and PM10 pollution in the Chinese population. *Environ. Res.* 136, 196–204. <https://doi.org/10.1016/j.envres.2014.06.029>.
- Madronich, S., Flocke, S., 1999. The role of solar radiation in atmospheric Chemistry. 1–26. https://doi.org/10.1007/978-3-540-69044-3_1.
- Manalisidis, I., Stavropoulou, E., Stavropoulos, A., Bezirtzoglou, E., 2020. Environmental and health impacts of air pollution: a review. *Front. Public Health* 8. <https://doi.org/10.3389/fpubh.2020.00014>.
- Oke, T.R., Mills, G., Christen, A., Voogt, J.A., 2017. *Urban Climates*. Cambridge University Press. <https://doi.org/10.1017/9781139016476>.
- Poliukhov, A., Chubarova, N., Kinne, S., Rivin, G., Shatunova, M., Tarasova, T., 2017. Comparison between calculations of shortwave radiation with different aerosol datasets and measured data at the MSU MO (Russia). In: AIP Conference Proceedings. AIP Publishing. <https://doi.org/10.1063/1.4975561>, 1810(1), 100006.
- Poliukhov, A.A., Chubarova, N.Ye., Volodin, E.M., 2022. Impact of inclusion of the indirect effects of sulfate aerosol on radiation and cloudiness in the INMCM model. *Izvestiya, Atmos. Oceanic Phys.* 58, 486–493. <https://doi.org/10.1134/S001433822050097>.
- Popovicheva, O.B., Evangelou, N., Eleftheriadis, K., Kalogridis, A.C., Sitnikov, N., Eckhardt, S., Stohl, A., 2017. Black carbon sources constrained by observations in the Russian High Arctic. *Environ. Sci. Technol.* 51, 3871–3879. <https://doi.org/10.1021/acs.est.6b05832>.
- Popovicheva, O., Chichaeva, M., Kovach, R., Zhdanova, E., Kasimov, N., 2022. Seasonal, weekly, and diurnal black carbon in Moscow megacity background under impact of urban and regional sources. *Atmosphere* 13, 563. <https://doi.org/10.3390/atmos13040563>.
- Pulles, T., van het Bolcher, M., Brand, R., Visschedijk, A., 2007. *Assessment of Global Emissions from Fuel Combustion in the Final Decades of the 20th Century*.
- Revich, B.A., 2018. Fine suspended particulates in ambient air and their health effects in megalopolises. *Probl. Ecol. Monit. Ecosyst. Model.* 29, 53–78. <https://doi.org/10.21513/0207-2564-2018-3-53-78>.
- Riemer, N., Vogel, H., Vogel, B., Fiedler, F., 2003. Modeling aerosols on the mesoscale-y: treatment of soot aerosol and its radiative effects. *J. Geophys. Res. Atmos.* 108 <https://doi.org/10.1029/2003JD003448>.
- Ritter, B., Geleyn, J.-F., 1992. A comprehensive radiation scheme for numerical weather prediction models with potential applications in climate simulations. *Mon. Weather Rev.* 120, 303–325. [https://doi.org/10.1175/1520-0493\(1992\)120<0303:ACRSFN>2.0.CO;2](https://doi.org/10.1175/1520-0493(1992)120<0303:ACRSFN>2.0.CO;2).
- Rivin, G.S., Vil'fand, R.M., Kiktev, D.B., Rozinkina, I.A., Tudriy, K.O., Blinov, D.V., Varentsov, M.I., Samsonov, T.E., Bundel', A.Yu., Kirsanov, A.A., Zakharchenko, D. I., 2019. The system for numerical prediction of weather events (including severe ones) for Moscow megacity: the prototype development. *Russ. Meteorol. Hydrol.* 44, 729–738. <https://doi.org/10.3103/S1068373919110025>.
- Rivin, G.S., Rozinkina, I.A., Vil'fand, R.M., Kiktev, D.B., Tudriy, K.O., Blinov, D.V., Varentsov, M.I., Zakharchenko, D.I., Samsonov, T.E., Repina, I.A., Artamonov, A. Yu., 2020. Development of the high-resolution operational system for numerical prediction of weather and severe weather events for the Moscow region. *Russ. Meteorol. Hydrol.* 45, 455–465. <https://doi.org/10.3103/S1068373920070018>.
- Royer, P., Chazette, P., Sartelet, K., Zhang, Q.J., Beekmann, M., Raut, J.-C., 2011. Comparison of lidar-derived PM10 with regional modeling and ground-based observations in the frame of MEGAPOLI experiment. *Atmos. Chem. Phys.* 11, 10705–10726. <https://doi.org/10.5194/acp-11-10705-2011>.
- Samsonov, T.E., Trigub, K.S., 2018. Mapping of local climate zones of Moscow city. *Geodesy Cartogr.* 936, 14–25. <https://doi.org/10.22389/0016-7126-2018-936-6-14-25>.
- Samsonov, T.E., Varentsov, M.I., 2020. Computation of City-descriptive parameters for high-resolution numerical weather prediction in Moscow megacity in the framework of the COSMO model. *Russ. Meteorol. Hydrol.* 45, 515–521. <https://doi.org/10.3103/S1068373920070079>.
- Schulz, J.-P., Vogel, G., 2020. Improving the processes in the land surface scheme TERRA: bare soil evaporation and skin temperature. *Atmosphere* 11, 513. <https://doi.org/10.3390/atmos11050513>.
- Schutgens, N., Sayer, A.M., Heckel, A., Hsu, C., Jethva, H., de Leeuw, G., Leonard, P.J.T., Levy, R.C., Lipponen, A., Lyapustin, A., North, P., Popp, T., Poulsen, C., Sawyer, V., Sogacheva, L., Thomas, G., Torres, O., Wang, Y., Kinne, S., Schulz, M., Stier, P., 2020. An AeroCom–AeroSat study: intercomparison of satellite AOD datasets for aerosol model evaluation. *Atmos. Chem. Phys.* 20, 12431–12457. <https://doi.org/10.5194/acp-20-12431-2020>.
- Shepelev, V., Glushkov, A., Slobodin, I., Cherkassov, Y., 2023. Measuring and modelling the concentration of vehicle-related PM2.5 and PM10 emissions based on neural networks. *Mathematics* 11, 1144. <https://doi.org/10.3390/math11051144>.
- Singh, R., Kumar, S., Singh, A., 2018. Elevated black carbon concentrations and atmospheric pollution around Singrauli coal-fired thermal power plants (India) using ground and satellite data. *Int. J. Environ. Res. Public Health* 15, 2472. <https://doi.org/10.3390/ijerph15112472>.
- Srimath, S.T.G., Sokhi, R., Karppinen, A., Singh, V., Kukkonen, J., 2017. Evaluation of an urban modelling system against three measurement campaigns in London and Birmingham. *Atmos. Pollut. Res.* 8, 38–55. <https://doi.org/10.1016/j.apr.2016.07.004>.
- Stewart, I.D., Oke, T.R., 2012. Local climate zones for urban temperature studies. *Bull. Am. Meteorol. Soc.* 93, 1879–1900. <https://doi.org/10.1175/BAMS-D-11-00019.1>.

- Stohl, A., Aamaas, B., Amann, M., Baker, L.H., Bellouin, N., Berntsen, T.K., Boucher, O., Cherian, R., Collins, W., Daskalakis, N., Dusinska, M., Eckhardt, S., Fuglestvedt, J.S., Harju, M., Heyes, C., Hodnebrog, Ø., Hao, J., Im, U., Kanakidou, M., Klimont, Z., Kupiainen, K., Law, K.S., Lund, M.T., Maas, R., MacIntosh, C.R., Myhre, G., Myriokefalitakis, S., Olivé, D., Quaas, J., Quennehen, B., Raut, J.-C., Rumbold, S.T., Samset, B.H., Schulz, M., Seland, Ø., Shine, K.P., Skeie, R.B., Wang, S., Yttri, K.E., Zhu, T., 2015. Evaluating the climate and air quality impacts of short-lived pollutants. *Atmos. Chem. Phys.* 15, 10529–10566. <https://doi.org/10.5194/acp-15-10529-2015>.
- Tegen, I., Hollrigl, P., Chin, M., Fung, I., Jacob, D., Penner, J., 1997. Contribution of different aerosol species to the global aerosol extinction optical thickness: estimates from model results. *J. Geophys. Res.-Atmos.* 102, 23895–23915. <https://doi.org/10.1029/97JD01864>.
- Tsikerdekis, A., Zanis, P., Georgoulas, A.K., Alexandri, G., Katragkou, E., Karacostas, T., Solmon, F., 2019. Direct and semi-direct radiative effect of North African dust in present and future regional climate simulations. *Clim. Dyn.* 53, 4311–4336. <https://doi.org/10.1007/s00382-019-04788-z>.
- Varentsov, M., Wouters, H., Platonov, V., Konstantinov, P., 2018. Megacity-induced Mesoclimatic effects in the lower atmosphere: a modeling study for multiple summers over Moscow, Russia. *Atmosphere* 9, 50. <https://doi.org/10.3390/atmos9020050>.
- Varentsov, M., Samsonov, T., Demuzere, M., 2020. Impact of urban canopy parameters on a Megacity's modelled thermal environment. *Atmosphere* 11, 1349. <https://doi.org/10.3390/atmos11121349>.
- Varentsov, M., Vasenev, V., Dvornikov, Y., Samsonov, T., Klimanova, O., 2023. Does size matter? Modelling the cooling effect of green infrastructures in a megacity during a heat wave. *Sci. Total Environ.* 902, 165966. <https://doi.org/10.1016/j.scitotenv.2023.165966>.
- Vil'fand, R.M., Kirsanov, A.A., Revokatova, A.P., Rivin, G.S., Surkova, G.V., 2017. Forecasting the transport and transformation of atmospheric pollutants with the COSMO-ART model. *Russ. Meteorol. Hydrol.* 42, 292–298. <https://doi.org/10.3103/S106837391705003X>.
- Vogel, B., Vogel, H., Bäumer, D., Bangert, M., Lundgren, K., Rinke, R., Stanelle, T., 2009. The comprehensive model system COSMO-ART – radiative impact of aerosols on the state of the atmosphere on the regional scale. *Atmos. Chem. Phys.* 9, 8661–8680. <https://doi.org/10.5194/acp-9-8661-2009>.
- Vogel, H., Bäumer, D., Bangert, M., Lundgren, K., Rinke, R., Stanelle, T., 2010. COSMO-ART: Aerosols and reactive trace gases within the COSMO model. In: *Integrated Systems of Meso-Meteorological and Chemical Transport Models*. Springer, Berlin, Heidelberg, pp. 75–80. https://doi.org/10.1007/978-3-642-13980-2_6.
- von Storch, H., Langenberg, H., Feser, F., 2000. A spectral nudging technique for dynamical downscaling purposes. *Mon. Weather Rev.* 128, 3664–3673. [https://doi.org/10.1175/1520-0493\(2000\)128<3664:ASNTFD>2.0.CO;2](https://doi.org/10.1175/1520-0493(2000)128<3664:ASNTFD>2.0.CO;2).
- Wang, Y., Le, T., Chen, G., Yung, Y.L., Su, H., Seinfeld, J.H., Jiang, J.H., 2020. Reduced European aerosol emissions suppress winter extremes over northern Eurasia. *Nat. Clim. Chang.* 10, 225–230. <https://doi.org/10.1038/s41558-020-0693-4>.
- Wouters, H., Demuzere, M., Blahak, U., Fortuniak, K., Maiheu, B., Camps, J., Tielemans, D., van Lipzig, N.P.M., 2016. The efficient urban canopy dependency parametrization (SURY) v1.0 for atmospheric modelling: description and application with the COSMO-CLM model for a Belgian summer. *Geosci. Model Dev.* 9, 3027–3054. <https://doi.org/10.5194/gmd-9-3027-2016>.
- Wu, D., Wu, C., Liao, B., Chen, H., Wu, M., Li, F., Tan, H., Deng, T., Li, H., Jiang, D., Yu, J.Z., 2013. Black carbon over the South China Sea and in various continental locations in South China. *Atmos. Chem. Phys.* 13, 12257–12270. <https://doi.org/10.5194/acp-13-12257-2013>.
- Yu, M., Tang, G., Yang, Y., Li, Q., Wang, Yonghong, Miao, S., Zhang, Y., Wang, Yuesi, 2020. The interaction between urbanization and aerosols during a typical winter haze event in Beijing. *Atmos. Chem. Phys.* 20, 9855–9870. <https://doi.org/10.5194/acp-20-9855-2020>.
- Zanaga, D., Van De Kerchove, R., De Keersmaecker, W., Souverijns, N., Brockmann, C., Quast, R., Wevers, J., Grosu, A., Paccini, A., Vergnaud, S., Cartus, O., Santoro, M., Fritz, S., Georgieva, I., Lesiv, M., Carter, S., Herold, M., Li, L., Tsendbazar, N.-E., Ramoino, F., Arino, O., 2021. ESA WorldCover 10m 2020 v100. Zenodo [data set]. <https://doi.org/10.5281/zenodo.5571936>.
- Zawadzka, O., Markowicz, K.M., Pietruczuk, A., Zielinski, T., Jaroslawski, J., 2013. Impact of urban pollution emitted in Warsaw on aerosol properties. *Atmos. Environ.* 69, 15–28. <https://doi.org/10.1016/j.atmosenv.2012.11.065>.
- Zhang, M., Jin, S., Ma, Y., Fan, R., Wang, L., Gong, W., Liu, B., 2021. Haze events at different levels in winters: a comprehensive study of meteorological factors, aerosol characteristics and direct radiative forcing in megacities of north and Central China. *Atmos. Environ.* 245, 118056. <https://doi.org/10.1016/j.atmosenv.2020.118056>.
- Zhdanova, E.Y., Chubarova, N.Y., Lyapustin, A.I., 2020. Assessment of urban aerosol pollution over the Moscow megacity by the MAIAC aerosol product. *Atmos. Meas. Tech.* 13, 877–891. <https://doi.org/10.5194/amt-13-877-2020>.
- Zhuang, B., Wang, T., Liu, J., Che, H., Han, Y., Fu, Y., Li, S., Xie, M., Li, M., Chen, P., Chen, H., Yang, X., Sun, J., 2018. The optical properties, physical properties and direct radiative forcing of urban columnar aerosols in the Yangtze River Delta, China. *Atmos. Chem. Phys.* 18, 1419–1436. <https://doi.org/10.5194/acp-18-1419-2018>.